INVESTIGATION OF WARPAGE AT FUSED DEPOSITION MODELING (FDM) PRINTED THERMOPLASTIC COMPOSITES

A THESIS SUBMITTED TO
THE SCHOOL OF GRADUATE STUDIES
OF
UNIVERSITY OF TURKISH AERONAUTICAL ASSOCIATION

BY

WILLIAM NDACYAYISENGA

IN PARTIAL FULFILLMENT OF THE REQUIREMENTS
FOR
THE DEGREE OF MASTER OF SCIENCE
IN
MECHANICAL AND AERONAUTICAL ENGINEERING

July 2024

INVESTIGATION OF WARPAGE AT FUSED DEPOSITION MODELING (FDM) PRINTED THERMOPLASTIC COMPOSITES

A THESIS SUBMITTED TO
THE SCHOOL OF GRADUATE STUDIES
OF
UNIVERSITY OF TURKISH AERONAUTICAL ASSOCIATION

BY

WILLIAM NDACYAYISENGA

IN PARTIAL FULFILLMENT OF THE REQUIREMENTS
FOR
THE DEGREE OF MASTER OF SCIENCE
IN
MECHANICAL AND AERONAUTICAL ENGINEERING

Supervisor: Assoc. Prof. Dr. Hamit TEKIN

July 2024

Approval of the thesis:

INVESTIGATION OF WARPAGE AT FUSED DEPOSITION MODELING (FDM) PRINTED THERMOPLASTIC COMPOSITES

submitted by **WILLIAM NDACYAYISENGA** in partial fulfillment of the requirements for the degree of Master of Science i**n** Mechanical and Aeronautical Engineering**, University of Turkish Aeronautical Association** by,

Assoc. Prof. Dr. Adnan GÜZEL
Dean, The School of Graduate Studies, UTAA _____

Assoc. Prof. Dr. Hamit TEKİN
Head of Department Mechanical and Aeronautical Engineering, UTAA _____

Assoc. Prof. Dr. Hamit TEKİN
Supervisor, Mechanical Engineering, UTAA _____

Examining Committee Members:

Assoc. Prof. Dr. Hamit TEKİN
Mechanical Engineering, UTAA _____

Assoc. Prof. Dr. İpek AYTAÇ
Mechanical Engineering, UTAA _____

Assoc. Prof. Dr. Ata HANLAR
Mechanical Engineering, Tarsus University _____

Date: 17.07.2024

I hereby declare that all information in this document has been obtained and presented in accordance with academic rules and ethical conduct. I also declare that, as required by these rules and conduct, I have fully cited and referenced all material and results that are not original to this work.

William, NDACYAYISENGA

Signature:

ABSTRACT

INVESTIGATION OF WARPAGE AT FUSED DEPOSITION MODELING (FDM) PRINTED THERMOPLASTIC COMPOSITES

NDACYAYISENGA, William
Master of Science, Mechanical and Aeronautical Engineering
Supervisor: Assoc. Prof. Dr. Hamit TEKİN

July 2024, 115 pages

Fused Deposition Modeling (FDM) is preferred among additive manufacturing techniques due to its applicability and the process cost. While FDM boasts versatility and material efficiency, one of its notable challenges is warpage, a phenomenon that adversely affects printed parts' dimensional stability and structural integrity. This study investigates the warpage on thin-walled L-shaped parts produced from carbon fiber-reinforced Polyamide-612 (PA612). This research primarily focuses on identifying the influence of FDM printing parameters, namely infill density, infill pattern, printing direction, and raster angle, on the occurrence of warpage in PA12-CF reinforced components. The study utilized MINITAB software to create an experimental design matrix. Through a general factorial design approach, the experimental design matrix involves 36 experiments. DIGIMAT-AM was used to simulate the warpage. The simulation results highlighted a range of warpage from a maximum of 4.5 mm to a minimum of 0.9 mm across the printed sample. The study also examined the deviation angle between features held by L shape-part, such as an electric motor and camera. The results showed a maximum deviation of 5.14º and a remarkable minimum deviation of 0.04º. These findings indicate that the geometrical errors due to Warpage can be controlled by strategically selecting printing parameters to minimize Warpage; the suitable parameters were infill density of 90%, infill pattern lines, printing direction Flat, and raster angle of 90°.

The outcomes of this research also indicated that the printed parts' tensile and flexural strength and stiffness are affected by the mentioned printing parameters. These findings contribute valuable knowledge towards advancing FDM technology by optimizing printing strategies for composite materials, thereby broadening its application spectrum across various sectors where the components' dimensional precision and structural integrity are critical.

July 17th, 2024.

Keywords: FDM, Warpage, Carbon fiber-reinforced PA612, Additive Manufacturing

ÖZ

HİBRİT ROBOTIK KOLU AKILLI KONTROLÜ

NDACYAYISENGA, William
Yüksek Lisans, Makina ve Uçak Mühendisliği
Tez Yöneticisi: Dr. Öğr. Üye. Hamit TEKİN

Temmuz 2024, 115 sayfa

Eriyik Yığma Modelleme (FDM), uygulanabilirliği ve proses maliyeti nedeniyle eklemeli imalat teknikleri arasında tercih edilmektedir. FDM çok yönlülüğü ve malzeme verimliliğiyle övünse de, dikkate değer zorluklarından biri de basılı parçaların boyutsal stabilitesini ve yapısal bütünlüğünü olumsuz yönde etkileyen bir olgu olan çarpıklıktır. Bu çalışma, karbon fiber takviyeli Polyamid-612'den (PA612) üretilen ince duvarlı L şeklindeki parçalar üzerindeki çarpıklığı araştırmaktadır. Bu araştırma öncelikle FDM yazdırma parametrelerinin, yani dolgu yoğunluğu, dolgu deseni, yazdırma yönü ve tarama açısının PA12-CF takviyeli filament ile basılan parçalarda çarpıklık oluşumu üzerindeki etkisini belirlemeye odaklanmaktadır. Çalışmada deneysel bir tasarım matrisi oluşturmak için MINITAB yazılımı kullanılmıştır. Çarpıklığı simüle etmek için DIGIMAT-AM yazılımı kullanıldı. Simülasyonlar için ince duvar L şeklinde bir örnek ele alındı. Sonuçlar parçada üretim parametrelerine göre maksimum 4,5 mm'den minimum 0,9 mm'ye kadar bir eğrilme aralığını oluşacağını gösterdi. Bu bulgular, çarpıklık nedeniyle oluşan geometrik hataların, yazdırma parametrelerinin stratejik olarak seçilmesiyle kontrol edilebileceğini göstermektedir. Bulgular, kompozit malzemeler için baskı stratejilerini optimize ederek FDM teknolojisinin geliştirilmesine yönelik değerli bilgilere katkıda bulunuyor ve böylece bileşenlerin boyutsal hassasiyetinin ve yapısal bütünlüğünün kritik olduğu çeşitli sektörlerde uygulama yelpazesini genişletiyor.

Anahtar Kelimeler: FDM, Warpage, Karbon fiberle güçlendirilmiş PA612, Katmanlı İmalat

Dedication

I want to thank the Government of Rwanda for its financial support and encouragement. I also want to thank my colleagues who developed views that helped in my thesis and the individuals who generously shared their abilities.

ACKNOWLEDGMENTS

First, I express my profound gratitude and appreciation to my supervisor, Assoc. Prof. Dr. Hamit TEKİN. Thank you for your help, suggestions, criticism, support, and insights throughout the research.

I am grateful to the Department of Mechanical and Aeronautical Engineering at the University of Turkish Aeronautical Association for their assistance and support and for providing vital information throughout the completion of this thesis.

I want to thank Seymanur Sirtli from the Department of Mechanical Engineering for her help and encouragement in completing my thesis.

I want to thank the technical team at the University of Turkish Aeronautical Association for their collaboration, assistance, and encouragement in completing this thesis.

TABLE OF CONTENTS

LIST OF TABLES

TABLES

LIST OF FIGURES

FIGURES

LIST OF ABBREVIATIONS

ABBREVIATIONS

FDM	Fused Deposition Modeling
AM	Additive Manufacturing
ABS	Acrylonitrile Butadiene Styrene
PLA	Poly Lactic Acid
TG	Glass Transition Temperature
CTE	Coefficient of Thermal Expansion
FFF	Fused Filament Fabrication
SLA	Stereolithographic
SLS	Selective Laser Sintering
PCA	Post Curing Apparatus
PC	Poly Carbonate
P-V	Probability Value
PMC	Polymer Matric Composite
FRC	Fiber-Reinforced Composite
SFRCs	Short Fiber-Reinforced Composites
CFRCs	Continuous Fiber-Reinforced Composites
ANOVA	Analysis of Variance
ASTM D638	American Standards Test Method
ASTM D790	American Standards Test Methods
UTS	Ultimate Tensile Strength
DOE	Design of Experiment

CHAPTER 1

INTRODUCTION

1.1 Introduction to Warpage at FDM

Additive manufacturing (AM) has become one of the most popular manufacturing techniques because it allows for the simple and cost-effective production of high-performance components. Among the AM techniques, Fused Deposition Modelling (FDM) is more essential because of its accessibility, low-cost production, and ability to build components utilizing multiple materials [1].

Fused deposition modeling is an AM technology that builds items layer by layer with thermoplastic polymers delivered via a heated nozzle that follows a predetermined path. Originally developed by Stratasys Inc., FDM has become one of the most popular and cost-effective processes for AM [2]. A key benefit of FDM is its capability to fabricate complex shapes [3]. Moreover, it doesn't require any tooling [4]. It facilitates extensive change, making small-scale production cost-effective. However, application in industry has been limited by various reasons, including the speed of construction, the mechanical qualities of the parts, and their dimensional precision [5].

The precision of FDM-produced objects is strongly dependent on the precise process parameters used. numerous recent studies have aimed to improve the quality of FDM-printed items [6]. One of the most serious challenges in FDM is the warpage. Warpage refers to distortion or deformation that occurs during and after 3D printing. During FDM printing, the material is deposed layer by layer. Each subsequent layer is slowly melted so that it can adhere to the layer below. As the material cools and solidifies, it contracts. This contraction may vary across the part due to variable cooling rates, resulting in internal tensions and warpage. Furthermore, the gradient air surrounding the printed item is the primary cause of warpage deformation [7],

Material properties and processing requirements both have an impact on warpage. Understanding how these material attributes affect warpage aids in the selection of materials and the control of printing settings to avoid this undesirable result [8].

Warpage can result in dimensional mistakes, rendering printed items unsuitable for applications requiring precision. In severe circumstances, warpage can cause pieces to detach from the build platform, resulting in print failure. This impacts the quality of printed goods, leads to material waste, and increases manufacturing time [9]. Warpage mainly focuses on creating large sculptures with thin walls or complex geometry. These parts are more prone to deformation due to uneven cooling and the associated forces. Furthermore, warpage can be a severe issue when scaling up 3D printing for mass production, where uniformity and accuracy are essential [10].

Warpage in FDM-printed composites is complex and varies depending on the material and printing conditions. Manufacturers may dramatically reduce warpage and increase the quality of 3D-printed parts by carefully selecting materials based on thermal expansion, glass transition temperature, moisture absorption, mechanical capability, and adhesive properties [11]. Adjusting printing parameters to meet specific material properties may also lessen warpage difficulties, resulting in outstanding printing results [12].

1.2 Aim and Objective of the Study

1.2.1 Aims

The aim of this research was to investigate the effects of infill shape and density on the warpage of FDM printed thermoplastic composites, which influence the dimensional accuracy of printed objects. In this research, the case study focused on determining the deviation angle between a thin-walled FDM printed camera holder and the camera itself, based on the printing process parameters.

1.2.2 Objectives

This study was meticulously designed to improve the quality and performance of 3D printed components created with PA12-CF polyamide 612, a solid and adaptable carbon fiber-reinforced polyamide material. The objectives of the study are:

- To minimize warpage
- To maximize the stiffness
- To maximize the flexural stiffness of the FDM printed composites by adjusting various process parameters such as infill density, infill pattern, printing direction, and raster angle.

1.3 The Outline of the Thesis

The thesis was divided into the following chapters:

Chapter One Context and Overview: This chapter introduces additive manufacturing, focusing on Fused Deposition Modeling (FDM). It outlines the research objectives and gives an overview of the thesis structure.

Chapter Two Introduction to Additive Manufacturing Technologies. This chapter covers FDM categories, mechanical principles of additive manufacturing, materials used, and a literature survey of FDM printed composites. It also addresses warpage and dimension accuracy, including process parameters affecting warpage and optimization of warpage.

Chapter Three Warpage Analysis: This chapter examines the effects of process parameters on the warpage and mechanical properties of FDM printed composites. It includes investigation, materials and sample preparation, geometry modeling, experimental setup, and Digimat-AM software simulation. It also discusses deviation angle and post-processing.

Chapter Four Experimental Analysis of Mechanical Properties: This chapter presents the results of tensile tests, mechanical characterization, and bending tests.

It includes sample preparation, design of experiment analysis using response surface methodology, and optimization of ultimate tensile strength and stiffness.

Chapter Five Conclusion: This final chapter discusses key findings and outcomes and suggests areas for future work. The thesis concludes with a comprehensive list of references, acknowledging the scholarly works and studies underpinning this research and framing it within the broader academic discourse on additive manufacturing. This structure facilitates a logical flow of information and ensures a thorough exploration of the intricate dynamics of Fused Deposition Modeling.

CHAPTER 2

LITERATURE REVIEW

2.1 Introduction to Additive Manufacturing Technologies

Additive Manufacturing (AM) is the method of making physical items from three-dimensional digital models by adding materials layer by layer. The method can be divided into three types: liquid-based, solid-based, and powder-based. Material jetting and photopolymerization are two liquid-based manufacturing procedures that require shaping objects in a liquid or viscous material condition before reinforcing them with heat [13]. Solid-based AM methods, on the other hand, use solid materials to form objects through processes such as fused deposition modeling and ultrasonic consolidation [14]. Finally, powder-based additive manufacturing technologies, such as powder bed fusion (PBF), use lasers or electron beams to melt and fuse material powders [15].

Some of the principal technologies integral to additive manufacturing, each suited to specific applications and materials, include:

- Stereolithography (SLA) is a cutting-edge 3D printing process that uses a laser to solidify liquid resin layers and create firm plastic.
- Selective Laser Sintering (SLS) uses a laser to solidify powdered materials such as nylon or polystyrene.
- Fused Deposition Modeling (FDM) creates models by melting thermoplastic material and layering it onto a print bed, similar to the extrusion method.

2.2 Stereolithography (SLA)

Stereolithography, created by 3D Systems in 1987 as the world's first commercial rapid prototyping system, has since grown into one of the most used methods. Figure 2.1 illustrates the stereolithographic equipment (SLA), which consists of a

construction platform (elevator) positioned within a vat of liquid monomer resin (either acrylic or epoxy resin), a recoating blade, and an ultraviolet helium-cadmium laser or argon ion laser [16].

The SLA procedure uses a laser beam to selectively cure the top layer of monomer resin, tracing the pattern explained by the sliced model. After a layer is formed, the platform goes deeper into the vat, and more liquid resin is added over the previously hardened layer, repeating the process until the item has been entirely manufactured. Once the piece is finished, it is raised off the platform, and any supporting structures are removed to reveal the "green" part. To harden the prototype, these green pieces are post-cured in a post-curing apparatus (PCA), which could be a controlled furnace or an ultraviolet oven [17]. The advantages of this method include a clean surface polish and high precision. However, the downsides are the high cost and toxicity of materials, the lengthy time required for post-processing, and the necessity for support structures, which might potentially damage surface smoothness when removed [18].

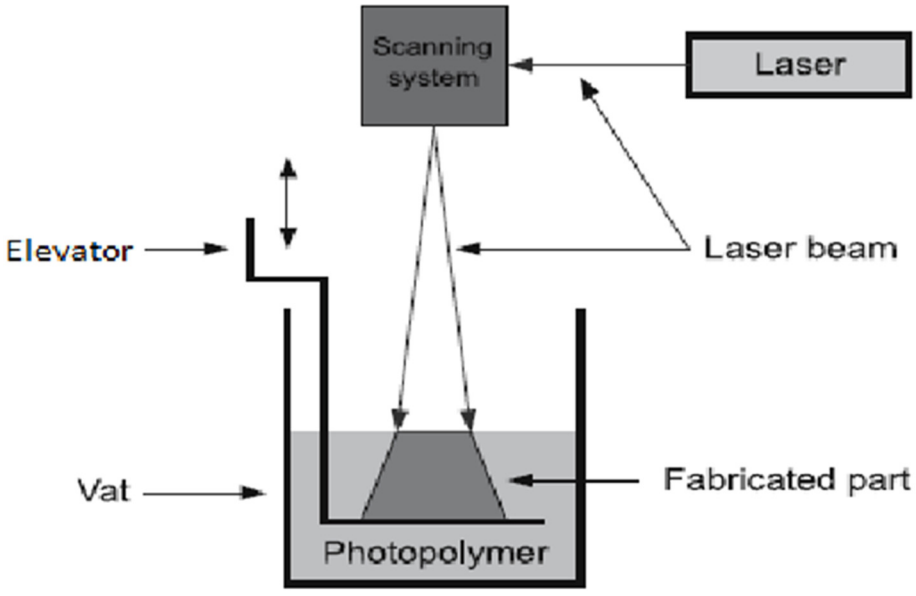

Figure 2.1: Schematic of the SLA Process [19]

- Similar to FDM, SLA printing requires supports to stabilize overhangs and undercuts and anchor the object to the build platform. These supports must be manually removed following processing. Because of SLA's precision, these

supports can be finer and less apparent, making them easier to remove while having less of an impact on the final part's surface.

- After completing an SLA print, it may need to be further processed. This includes washing in a solvent to remove any uncured resin, followed by post-curing under UV light to ensure complete curing and improve the material's mechanical qualities. Support removal and surface finishing may also be required, depending on the application.
- The precision and accuracy of SLA are controlled by the laser's spot size (typically ranging from 100 to 140 microns in diameter) and the precision of the galvanometer mirrors. The smaller the spot size and the more precise the mirror movements, the finer details can be achieved in the printed parts.
- SLA materials are diverse, ranging from rigid to flexible, and can mimic various engineering plastics. However, they generally tend to be more brittle than those produced by other manufacturing methods. This limits their use in functional applications requiring high mechanical strength or thermal stability.

2.3 Selective Laser Sintering (SLS)

The University of Texas at Austin developed selective laser sintering (SLS) technology, which was later commercialized by DTM Corporation. It is popular because it can produce parts without the requirement for support structures and may use any number of powder materials, including polycarbonate (PC), nylon, nylon/glass composite, wax, ceramics, correct form (TM), and elastomeric and metal-polymer powders [20].

Modern SLS technique melts and fuses powdered materials using a CO2 laser beam. A roller transfers a small amount of powder to the build surface, which is heated slightly below its melting point. The laser then selectively sinters the powder according to the part's cross-sectional design, resulting in the layer shown in Figure 2.2. The process continues with varying amounts of powder until the part is complete.

The advantages of this technology include the use of a wide range of thermoplastic powders, simple post-processing, and the elimination of the requirement for support structures. However, it is essential to note that the surface polish of sintered models may be rough, and the higher cost of the technique may be seen as a disadvantage [21].

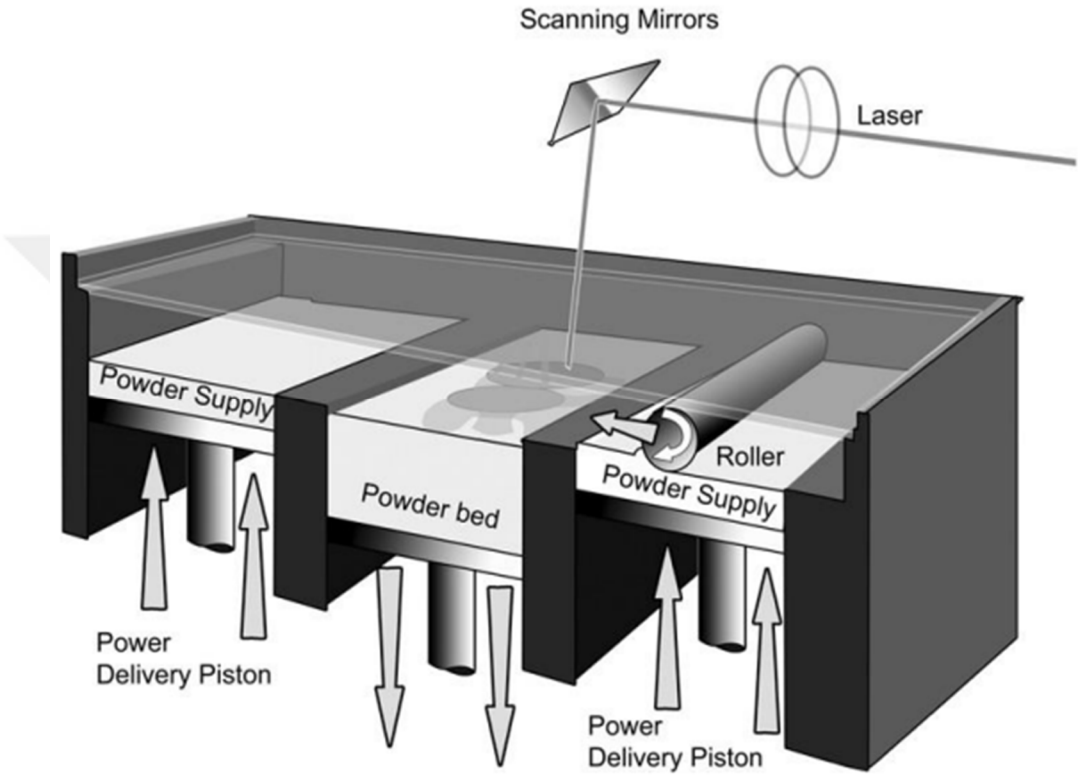

Figure 2.2: Schematic of the SLS Process [22]

SLS diminishes the need for supporting structures. The not-sintered powder can support complex geometries and overhangs, allowing elaborate designs and internal pieces to be manufactured without requiring additional post-processing to remove supports. This greatly enhances the production of complex parts and assemblies.

After printing, SLS parts often get covered in non-sintered powder and must be cleaned. Brushing off loose powder and bead blasting are popular post-processing methods for improving surface finish.

Additional processes, such as dyeing, sealing, or material penetration, can enhance the mechanical visual qualities of the components.

2.4 Fused Deposition Modeling (FDM)

In 1991, Stratasys developed fused deposition modeling, or FDM, as a means of rapid prototyping. It is the second most widely used technology, behind stereolithography. This method entails feeding plastic filament from a coil into an extrusion nozzle head controlled by a processor and depositing the material in thin layers on a platform.

The nozzle tip heats up to melt the plastic and features a mechanism for controlling the flow of the molten plastic. The FDM machine works similarly to an XY plotter. It uses a small nozzle to extrude thermoplastic filament onto a platform layer by layer. The platform offers cool temperatures, so the extruded material hardens quickly [23].

Each functioning layer connects with and solidifies the layer behind it. Figure 2.3 illustrates that modern FDM machines include two nozzles: one for the primary material and one for the support material. After the object has been fabricated, the support structures are removed for final processing. FDM can work with a variety of modeling materials and colors, including standard and medical-grade acrylonitrile butadiene styrene, elastomer, polycarbonate, polyphenylsulfone, and investment casting wax [24]. The advantages of this technology include the small size of the FDM machines, the ability to sterilize models, and enhanced geometric precision. However, downsides include lengthier production times and inferior surface quality when compared to stereolithography [25].

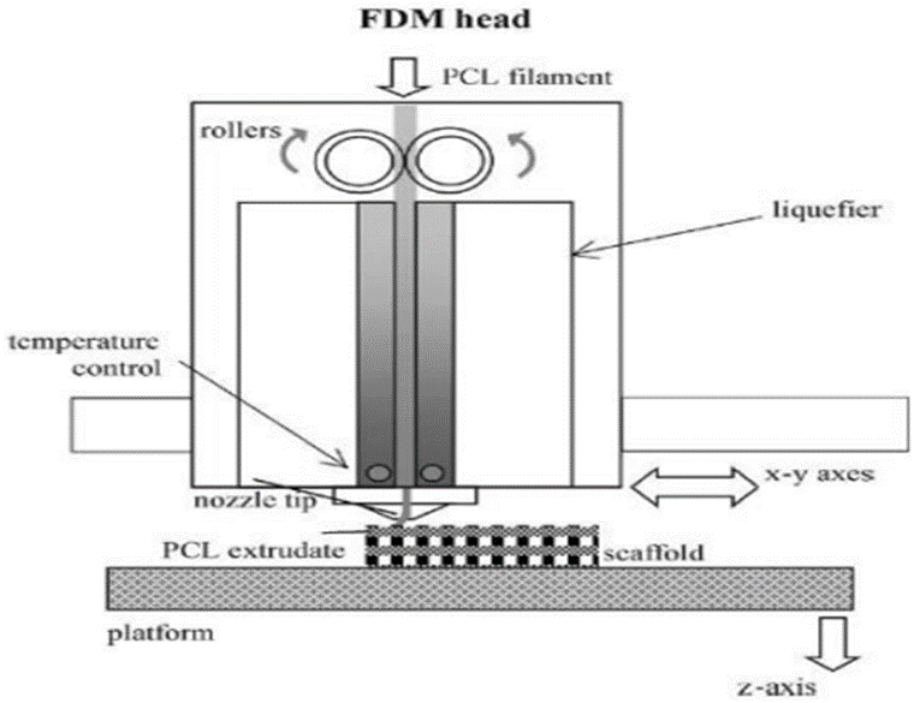

Figure 2.3: Schematic of the FDM Process [26]

The mechanical principles of FDM rely on multiple crucial components and processes working together to build parts directly from a digital model [27]. The following details encapsulate the mechanical principles that govern the FDM process:

- Material Extrusion and Heating: The core mechanism of FDM involves extruding thermoplastic material, typically supplied as a filament on a spool. Materials such as ABS, PLA, or nylon are pushed by a drive gear into an extruder that leads to a heated nozzle. The nozzle temperature is critical and finely adjusted to melt the filament just prior to extrusion. The appropriate melting temperature varies by material and is crucial for ensuring smooth flow without degrading the material.
- Layer-by-Layer Deposition: Fine strands of molten material are extruded and put down on the construction platform or on top of previous layers. The printer nozzle moves in accordance with the X and Y coordinates provided by G-code, which are obtained from the part's 3D model. As the substance is applied, it immediately cools and solidifies, sticking to the layer below. Following each layer, the build

platform normally adjusts vertically (Z direction) to prepare for the deposition of the following layer. This cycle continues until the thing is fully constructed.

- Temperature Management: Effective temperature control is crucial in FDM to ensure strong layer adhesion and minimize warping or distortions in the final product. This includes managing the nozzle's temperature and potentially heating the build platform to keep the lower layers from cooling too rapidly. A heated platform helps maintain a consistent temperature throughout the part during the print, reducing internal stresses that could cause warping or layers to separate.
- Path Planning and G-code Execution: The path for depositing the melted filament is meticulously calculated by slicing software, which transforms the 3D model into layers and generates G-code for movement paths. This G-code is essential, as it dictates the printer's movements, material flow rates, and temperatures, directly influencing the finish, strength, and dimensional accuracy of the final part.
- After deposition, the material must cool and solidify to support additional layers. Most FDM machines have cooling fans that aid expedite the deposition process. The pace of cooling can change the crystallinity and internal tensions in the material, influencing the mechanical qualities of the completed product.
- FDM printers may require temporary support structures for overhanging sections and complex geometries. These structures can be manufactured of easily removable materials. These supports are critical for maintaining the part's integrity during printing, but removing them requires additional effort in post-processing.

2.5 Materials Used in Additive Manufacturing

Additive Manufacturing combines various technologies to work with a wide variety of materials. The materials employed have an essential effect on the output's effectiveness and quality because each is chosen based on its individual characteristics and intended application.

This introduction evaluates some of the most commonly used materials in additive manufacturing, including ABS, PLA, and Nylon, along with their requirements and drawbacks [28].

Advantages of ABS include:

- High availability and low cost
- Longer lifespan compared to Nylon.
- Available in various colors.
- Effective for creating prototypes and models.

Disadvantages of ABS:

- Requires a closed printing platform to avoid warping.
- Non-biodegradable, making disposal difficult.
- Emits toxic fumes and odors at high temperatures.

PLA, or Polylactic Acid, is another plastic used in FDM. It melts at a lower temperature than ABS, simplifying the printing process but limiting its use in high-temperature applications. PLA is favored among hobbyists and for educational purposes because it is easy to use, provides a good surface finish, and minimizes warping. It is biodegradable and derived from renewable resources like corn starch [29].

Advantages of PLA:

- Simpler to print with.
- Available in a wide array of colors.
- Suitable for printing designs with sharp edges.

Disadvantages of PLA:

- Susceptible to deformation under high heat.
- The materials produced are not very robust.

Nylon, used in Selective Laser Sintering (SLS) and FDM, is ideal for engineering applications requiring durable, functional parts and tools.

It offers excellent strength, flexibility, resistance to wear and impact, and good thermal properties. Nylon's capacity to absorb moisture can impact its stability and mechanical characteristics, necessitating careful storage and handling. Although it can be challenging to print due to tendencies to string and warp, with proper settings and environmental control, Nylon can be very effective [4].

Advantages of Nylon:

- Extremely durable and flexible.
- Ideal for replacing traditional injection molding.
- Possesses excellent mechanical properties for various applications.
- Can be colored, dyed, tumbled, and smoothed quickly.

Disadvantages of Nylon:

- Potential shrinkage due to temperature variations.
- SLS post-processing can be complex.
- Long cooling periods may affect productivity.
- Nylon filaments for FDM and FFF require thorough drying for optimal results.

2.6 Fiber-Reinforced Thermoplastics for FDM

Composites are engineered materials that blend various components to improve their overall valuable qualities. Composite materials are used in 3D printing to increase mechanical qualities and specific optical, thermal, and electrical capabilities that pure polymers cannot achieve independently. A composite material typically consists of one or more reinforcing elements contained in a matrix or binder [30]. To attain desired functional qualities or combinations thereof, FDM-printed composites can be reinforced using various materials. Particles, fibers, and nanomaterials can be used as reinforcement to create polymer matrix composites (PMC). PMCs used in 3D printing include micro- or nanocomposites, metal particle-reinforced composites,

and short or continuous fiber-reinforced composites, with the latter being the most prominent [31].

Short or continuous fiber reinforcements are favored in PMC due to their excellent strength-to-weight ratios, enhanced rigidity, and corrosion resistance [32]. This section investigates fiber-reinforced composites in the FDM process, focusing on fiber reinforcements, including synthetic, high-performance man-made fibers and natural cellulose fibers. The desired qualities of the final composite influence the fiber type selection. High-performance fibers like carbon, glass, and Kevlar are extensively used, and natural fibers like flax, basalt, jute, and bamboo are gaining popularity in the FDM composites market [33]. The following sections will discuss the complexities of short and continuous fiber-reinforced composites and their qualities, advantages, and potential applications.

2.7 Short Fiber-Reinforced Composites

Short fiber-reinforced composites (SFRCs) serve an essential role in additive manufacturing (AM) by improving the material properties of printed items. They strike the right balance of performance, efficiency, and processing ease of use. These composites are made up of a polymer matrix reinforced by short fibers of glass, carbon, or aramid that are randomly oriented inside it. This reinforcement improves the underlying polymer's tensile, thermal, and geometrical qualities, allowing SFRCs to be used in various industries and applications.

The primary purpose of short fiber reinforcement in polymers is to improve the strength of 3D-printed components. Pure polymer parts typically lack enough strength, limiting their use in industrial applications [34].

Short Fiber Reinforced Composites (SFRCs) play a vital role in Additive Manufacturing (AM) by improving the mechanical properties of printed objects. The introduction of short fibers into polymers increases tensile strength, impact resistance, and stiffness, making SFRCs suitable for high-stress applications requiring significant load-bearing capacity and durability.

Short fibers also improve thermal stability and heat resistance in composites, which is useful when components are subjected to high thermal loads or need to maintain dimensional stability at high temperatures [35]. Furthermore, by changing the kind and quantity of fibers, the thermal conductivity of the composite may be modified, simplifying specific heat management requirements in applications such as electronic casings or automotive parts [33].

According to the findings of Ning et al. [36], repoted that short fibers often increase a polymer matrix's tensile strength and Young's modulus, but they can reduce toughness, ductility, and yield strength. Li et al. studied the influence of introducing short carbon fibers to a PEEK polymer matrix, using samples printed in both vertical and horizontal orientations [37]. The vertical position demonstrated increased flexural strength and modulus. Furthermore, Zhang et al. discovered that adding short CF to the ABS matrix increased the print's porosity, which may have reduced its strength.

Ding et al [38] was carried out to study the effect of printing orientation, layer thickness, and printing temperature on a CF/PLA composite manufactured using the FDM method. The specimens' orientation improves clarity.

The findings revealed that specimens printed with a 0° fiber orientation had greater tensile strength than specimens printed with a 90° orientation. The difference in strength between 0° and 90° fiber orientations is due to how they support the tensile load. When the fiber orientation is 0°, the tensile strength of the specimen is mostly determined by its CF strength.

2.7.1 Advantages and Disadvantages of Short Fibre Reinforced Composites

Short fiber reinforced composites (SFRCs) have become popular in additive manufacturing (AM) due to their ability to enhance printed parts' mechanical properties and durability. These composites comprise a polymer matrix with short embedded fibers that can be created from materials like glass, carbon, or aramid. During the printing process, the short fibers, usually less than one millimeter in length,

are randomly arranged within the polymer matrix. The use of SFRCs in AM provides several advantages and disadvantages [39].

Advantages:

- Enhanced Mechanical Properties: Adding short fibers to the polymer matrix significantly enhances its mechanical strength, stiffness, and impact resistance. This makes SFRCs ideal for applications requiring robust and durable parts.
- Improved Thermal Properties: SFRCs exhibit better thermal stability and heat resistance than their unreinforced counterparts. This property is crucial for applications exposed to high temperatures or requiring good dimensional stability under thermal stress.
- Cost-Effectiveness: Short fibers are generally less expensive and simpler to integrate into existing manufacturing processes than continuous fiber composites. This makes SFRCs a more economical option for strengthening 3D-printed parts without significantly increasing costs.
- Increased Design Flexibility: The random orientation of short fibers within the matrix allows for more uniform material properties in all directions, unlike continuous fiber composites that are anisotropic. This isotropy can be particularly advantageous in complex geometries with unpredictable directional loading conditions.
- Ease of Processing: SFRCs can be easier to process in AM than continuous fibers because they do not require complex mechanisms to lay fibers in specific orientations. This simplifies the printing process and reduces the risk of nozzle clogging.

Disadvantages:

- Limited Fiber Alignment Control: One of the main disadvantages of SFRCs is the lack of control over fiber orientation. Since the fibers are randomly distributed, achieving the directional strength and stiffness that oriented or continuous fibers provide is challenging.

- Reduced Performance Compared to Continuous Fibers: While SFRCs enhance material properties compared to unreinforced plastics, they generally do not reach the same performance level as continuous fiber composites, particularly in terms of tensile strength and modulus.
- Material Complexity and Handling: Mixing and handling short fiber composites can be more complex than dealing with homogenous materials. The fibers must be evenly dispersed within the matrix, requiring specialized equipment and techniques.
- Print Quality Issues: The presence of fibers can sometimes lead to issues with surface finish and detail resolution in the printed parts. Fibers may also cause frequent nozzle clogging, particularly with higher fiber loadings or if they are not adequately processed.
- Post-Processing Requirements: Parts made from SFRCs Often require more post-processing, such as additional curing or surface treatments, to achieve the desired material properties and surface quality.

2.8 Continuous Fibre-Reinforced Composites

Continuous fiber-reinforced composites, or CFRCs, have altered additive manufacturing (AM) by expanding their capabilities and applications. During 3D printing, continuous fibers like carbon, glass, or aramid are deposited into a thermoplastic or thermoset matrix. The end result is a composite material that greatly improves the mechanical characteristics, toughness, and utility of printed products. CFRCs considerably improve printed items' mechanical qualities, particularly strength, stiffness, and load-bearing capacity. Continuous fibers' excellent tensile strength and fatigue resilience allow for the production of lightweight components with strength equivalent to metals [40].

Frank van der Klift et al. [41] experimented sing a Nylon matrix and CF, they discovered that adding fibers increased tensile strength while increasing vacancy content, resulting in a low tensile modulus. Caminero et al. [42] Charpy impact

experiments were conducted on continuous fiber-reinforced composites made of glass, Kevlar, and carbon. They discovered that increasing the fiber volume percentage increased impact strength, and an on-edge orientation outperformed a flat orientation. Impact strength, microstructural analysis, print orientation, and fiber volume fraction (FVF).

A dual extruder can produce continuous fiber-reinforced composites (CFRC). Continuous fiber-reinforced composites (CFRC) can be manufactured by either co-extrusion [43] or dual extrusion [44] method. For this procedure, the FDM print machine head receives fiber filaments and thermoplastic resin on distinct occasions. The heated nozzle melts the thermoplastic filament, allowing the resin to saturate the reinforcing fiber as it flows through. When the resin-covered fiber is extruded to the nozzle and placed on the printing platform, the extruded filament adheres to the layer before it and hardens [45]. The dual extrusion procedure uses two nozzles to extrude the thermoplastic resin filament and reinforce the fiber filament separately on the printing plate. Figure 2.4a depicts a standard FDM printing process, whereas Figure 2.4b and 2.4c show schematic diagrams for co-extrusion and dual extrusion, respectively.

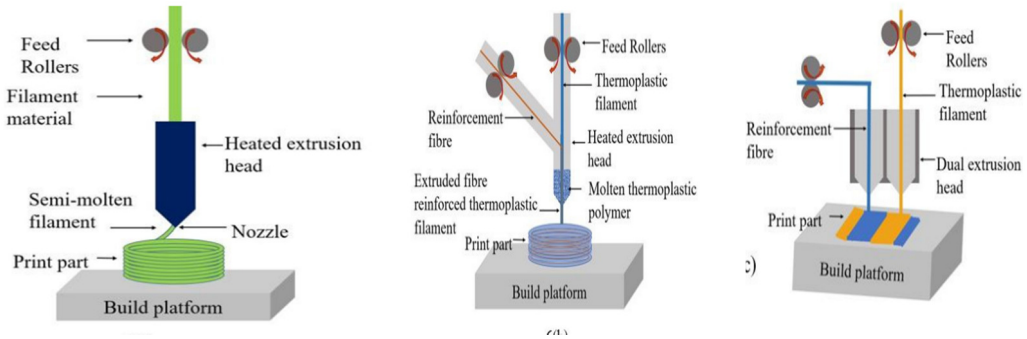

(a) (b) (c)

Figure 2.4: (a) Common FDM printer for polymers and short fiber-reinforced composites (SFRC). (b) Co-extrusion FDM printer for continuous fiber-reinforced composites (CFRC). (C) Dual-Extrusion FDM printer for CFRC [46]

2.8.1 Advantages and Disadvantages of Continuous Fiber Reinforced Composites

Continuous fiber-reinforced composites (CFRCs) are gaining popularity in additive manufacturing (AM) due to their excellent mechanical qualities and flexibility to high-performance applications. Despite their promise, there are both advantages and challenges to using them [47].

Advantages:

- Continuous fibers like carbon, glass, or aramid improve mechanical strength and stiffness in composites. CFRCs have great strength and stiffness, making them excellent for applications that demand robust mechanical performance, such as aerospace and automotive parts.
- High Load Bearing Capacity: Due to their high strength-to-weight ratio, CFRCs are ideal for structural applications where weight savings are critical. This aspect is precious in sectors like aerospace, where every gram of weight reduction can lead to significant fuel savings and performance enhancements.
- Superior Durability and Toughness: CFRCs offer improved durability and impact resistance compared to many other materials used in AM. This makes them suitable for producing parts exposed to demanding operational conditions over extended periods.
- Tailored Properties: One key benefit of using CFRCs in AM is controlling fiber orientation and volume fraction. This allows for tailoring mechanical and thermal properties to specific application needs, optimizing the part's performance depending on the directional stresses it will encounter.
- Thermal Stability: Continuous fibers improve the thermal stability of the composite, reducing the likelihood of deformation under heat exposure. This is critical for parts that operate in high-temperature environments or are subjected to wide temperature variations.

Disadvantages:

- Complexity in Manufacturing: Integrating continuous fibers into additive manufacturing processes is technically challenging. The placement, orientation, and impregnation of fibers require precise control, making the process complex and sometimes limiting the geometrical freedom typically associated with AM.
- Higher Material and Processing Costs: CFRCs generally involve higher material costs than standard thermoplastics or short fiber composites. The specialized equipment and additional process control needed can also increase manufacturing costs.
- Limited Material Availability: Compared to other AM materials, the range of composite materials that can be effectively used with continuous fibers is still relatively limited. This can restrict design choices and applications.
- Difficulty in Achieving Homogeneous Properties: While the ability to tailor properties is advantageous, it also comes with the challenge of achieving uniform material properties throughout the part. Variations in fiber distribution and orientation can lead to anisotropy, which might be undesirable in some applications.
- Post-Processing Requirements: Parts made from CFRCs often require significant post-processing, including machining, surface finishing, and sometimes curing or annealing to achieve the desired mechanical properties and dimensions.

2.9 Optimization of Warpage

To optimize and control Warpage, several strategies can be implemented [27]:

- Material Selection: Choosing materials with lower coefficients of thermal expansion (CTE) can inherently reduce the tendency to warp.
- Part Orientation: Orienting parts in a way that minimizes large flat areas exposed to high thermal gradients can significantly reduce warpage.
- Use of Rafts and Brims: Adding a raft or brim can improve adhesion to the build platform and distribute the stresses more evenly, reducing the effects of warpage.

- Post-Processing: Techniques like annealing (controlled heating) post-printing can relieve internal stresses and reduce warpage.
- Software Simulation: Advanced slicing software now includes simulation tools that predict warpage, allowing users to adjust parameters before printing to minimize effects.

CHAPTER 3

WARPAGE ANALYSIS

3.1 Investigation of The Effects of Process Parameters on Warpage and Mechanical Properties of FDM Printed Composites

3.1.1 Introduction

This study examines the impact of infill density, infill pattern, printing direction, and raster angle on the dimensional accuracy of printed objects. It explores the effects of each parameter on Warpage and recommends fine-tuning FDM methods to increase print quality.

3.2 Material

3.2.1 Materials and Sample Preparation

The material utilized in this thesis was carbon fiber-reinforced Polyamide 612. This particular filament contains 15% carbon fiber by weight. Polyamide PA12 absorbs less moisture than other polyamides, such as PA6 or PA66. Additionally, PA612 helps absorb and distribute stresses evenly throughout the material, reducing the potential for warpage.

3.2.2 Geometry Model in Solidworks

This study investigates the effect of the FDM printing parameters on the dimensional accuracy of thin-walled components. As a case study, the warpage issue was investigated using DIGIMAT AM in a thin-walled L-shape part Figure 3.1 camera holder of a gimbal integrated into an unmanned aerial vehicle.

The camera holder's 3D model was designed using SOLIDWORKS software. The camera's dimensions were taken to create the 3D model in SOLIDWORKS (Figure 3.1), which was then exported as a stereolithographic (STL) file.

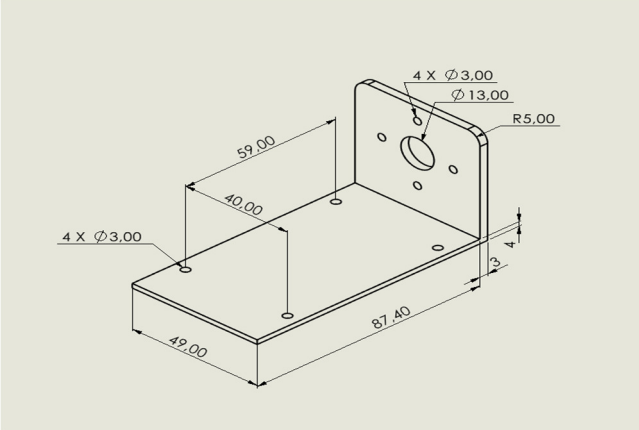

Figure 3.1: The camera holder

3.3 Experimental set-Up

3.3.1 Sample Preparation

The samples were printed on a Raise3D E2CF machine using PA12-CF carbon fiber reinforced composite filament. The Raise3D E2CF 3D printer was specifically built and optimized for manufacturing carbon fiber-reinforced filaments and other composite materials. Because the fiber-reinforced filaments are abrasive, the extruder required a robust steel nozzle with a diameter of 0.4 mm. The infill layer had a shell thickness of 0.8 mm, a print speed of 80 mm/s, and a layer height of 0.1 mm. The build plate temperature was set at 60 °C, the printing nozzle at 280 °C, and the chamber temperature was measured as 28 °C. The printing took place without the use of any glue. After determining the process and experiment settings, the models were configured using the slicing tool IDEAMAKER 4.3.1, the G-codes were transmitted to the printer, and the samples were printed. Figure 3.2 shows the part's measurements and printing orientation.

Figure 3.2: 3D Printed

3.4 Design of Experiment (DOE) For Warpage

This study seeks to analyze the warpage of a printed part by examining various aspects such as infill percentage (25%, 50%, and 90%), infill pattern (Lines,

Concentric, and Triangles), printing direction (Flat and on-edge), and raster angle (45 and 90°).

To do this, a factorial design approach was utilized to create an experimental design matrix for the four components, each having various levels. A total of 36 tests were run using the design matrix. The MINITAB 21.1.0 statistical program was used to examine the results. Tables 3.1 and 3.2 show four process parameters, their levels, and a design matrix.

Table 3.1: Fabrication parameter

Run	Infill density (%)	Infill pattern	Printing direction	Raster angle (Degrees)
1	25%	Lines	Flat	45
2	50%	Concentric	On edge	90
3	90%	Triangles		

Table 3.2: Representation of 36tests design matrix

Run	Infill density	Infill pattern	Printing direction	Raster angle
1	25	Lines	Flat	45
2	25	Lines	Flat	90
3	25	Lines	On edge	45
4	25	Lines	On edge	90
5	25	Concentric	Flat	45
6	25	Concentric	Flat	90
7	25	Concentric	On edge	45
8	25	Concentric	On edge	90
9	25	Triangles	Flat	45
10	25	Triangles	Flat	90
11	25	Triangles	On edge	45
12	25	Triangles	On edge	90
13	50	Lines	Flat	45
14	50	Lines	Flat	90
15	50	Lines	On edge	45
16	50	Lines	On edge	90
17	50	Concentric	Flat	45
18	50	Concentric	Flat	90
19	50	Concentric	On edge	45
20	50	Concentric	On edge	90
21	50	Triangles	Flat	45
22	50	Triangles	Flat	90
23	50	Triangles	On edge	45

24	50	Triangles	On edge	90
25	90	Lines	Flat	45
26	90	Lines	Flat	90
27	90	Lines	On edge	45
28	90	Lines	On edge	90
29	90	Concentric	Flat	45
30	90	Concentric	Flat	90
31	90	Concentric	On edge	45
32	90	Concentric	On edge	90
33	90	Triangles	Flat	45
34	90	Triangles	Flat	90
35	90	Triangles	On edge	45
36	90	Triangles	On edge	90

3.5 Simulation of The Warpage

The simulation of warpage involves utilizing computational methods and software tools to predict and analyze the deformation of parts due to thermal stress, material shrinkage, and other factors during and after the manufacturing process.

The STL model was sliced with the Ultimaker slicer for warpage simulation, and the resulting G-code was exported into DIGIMAT AM. The model was then rebuilt in DIGIMAT AM, taking into account the direction of the filaments at each layer. In addition, material properties such as fiber reinforcement and orientation, as well as FFF process characteristics such as extruder and chamber temperature, were taken into account during printing. In the definition step, the Fused Filament Fabrication (FFF) manufacturing process was chosen, which uses a generic FFF printer with a chamber size of 607 mm (X) x 596 mm (Y) x 465 mm (Z) and a fixed platform. The analysis type chosen was warpage-high-fidelity. The analysis was performed using a mesh size coefficient of 0.855 and 30566 voxels. The orientation of the carbon fibers data was obtained from Yu et al. in 2019 [48].

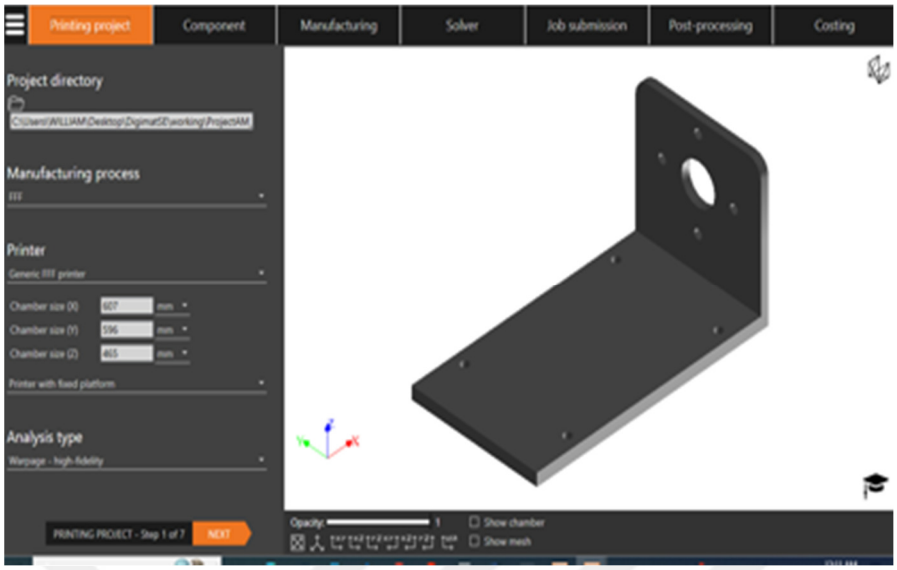

Figure 3.3: The printing project and its chamber size

Following data input, the DIGIMAT-AM software's required production parameters were determined. The chamber temperature was adjusted to 28°C, the extrusion temperature to 280°C, the build plate temperature to 60°C, the bead width to 0.5mm, and the convection coefficient to 0.015 mW/(mm2.°C). After reaching a final temperature of 25°C and a room temperature of 23°C, the cooling period was set to 30 minutes.

Table 3.3: Process parameters for simulations

Process parameters	Values	Unit
Chamber temperature	28	°C
Extrusion temperature	280	°C
Build plate temperature	60	°C
Bead width	0.5	mm
Convection coefficient	0.015	mW/ (mm2. °C)
Cooling time	30	min
Final temperature	25	°C
Room temperature	23	°C

3.6 Simulation of The Deviation Angle

The research studies the deviation angle between features held by L-shaped parts, including an electric motor and a camera, to ensure high manufacturing quality and geometric accuracy. The study used SolidWorks software to measure the deviation angle caused by the warpage.

Figure 3.4: Desired assembly orientation

The deviation angle, which measures the angle between the intended design features and the actual printed result, is a crucial aspect that warpage can significantly affect.

Figure 3.5 depicts the deviation angle with print direction on flat and edge surfaces, using 45 and 90° raster angles. The study utilized a 25% infill density and a line infill design.

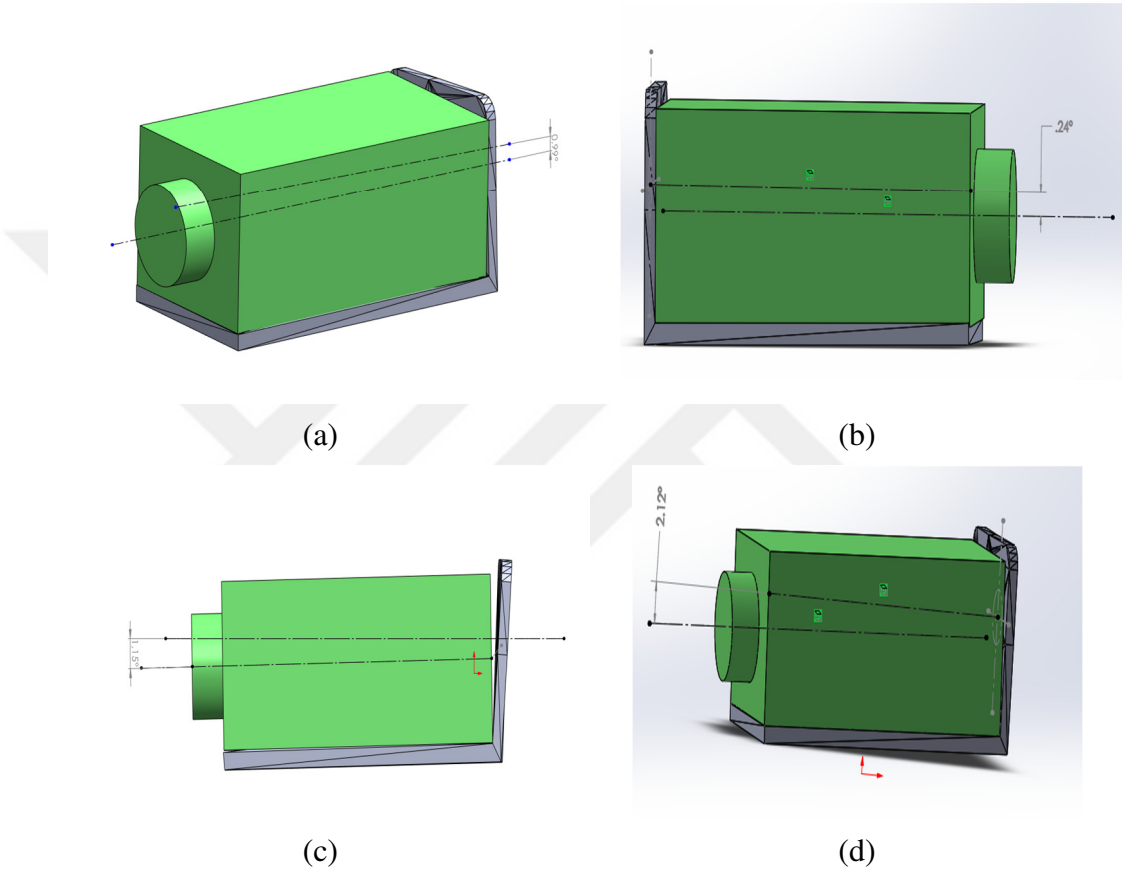

(a) (b)

(c) (d)

Figure 3.5: The results of deviation angle by infill density 25%, infill pattern is lines with printing direction: a) Flat 45° b) flat 90° c) on edge 45° d) on edge 90°

3.7 The Results of Warpage and Deviation Angle Analyses

The results of warpage and deviation angle analyses are presented in Table 3.4

Table 3.4: Results of warpage in all 36 tests and deviation angle

Run	Infill density	Infill pattern	Printing direction	Raster angle	Warpage (mm)	Deviation angle(Degree)
1	25	Lines	Flat	45	2.175	0.99
2	25	Lines	Flat	90	0.9755	0.24
3	25	Lines	On edge	45	2.563	1.15
4	25	Lines	On edge	90	1.452	2.12
5	25	Concentric	Flat	45	2.046	1.81
6	25	Concentric	Flat	90	1.062	1.71
7	25	Concentric	On edge	45	2.017	0.62
8	25	Concentric	On edge	90	1.882	4.42
9	25	Triangles	Flat	45	2.03	0.83
10	25	Triangles	Flat	90	0.9855	0.45
11	25	Triangles	On edge	45	1.79	0.49
12	25	Triangles	On edge	90	1.472	0.04
13	50	Lines	Flat	45	1.576	1.45
14	50	Lines	Flat	90	0.9142	0.8
15	50	Lines	On edge	45	2.866	1.21
16	50	Lines	On edge	90	1.663	2.42
17	50	Concentric	Flat	45	1.91	1.14
18	50	Concentric	Flat	90	1.136	1.75
19	50	Concentric	On edge	45	1.646	0.5
20	50	Concentric	On edge	90	1.511	0.47
21	50	Triangles	Flat	45	2.002	1.11
22	50	Triangles	Flat	90	0.9523	2.75
23	50	Triangles	On edge	45	3.312	1.56
24	50	Triangles	On edge	90	1.452	0.16
25	90	Lines	Flat	45	1.641	1.66
26	90	Lines	Flat	90	0.9094	0.49
27	90	Lines	On edge	45	3.784	1.7
28	90	Lines	On edge	90	1.634	0.74
29	90	Concentric	Flat	45	1.969	1.04
30	90	Concentric	Flat	90	0.9976	1.56
31	90	Concentric	On edge	45	1.850	0.43
32	90	Concentric	On edge	90	1.516	0.24
33	90	Triangles	Flat	45	1.652	1.38
34	90	Triangles	Flat	90	0.9304	1.28
35	90	Triangles	On edge	45	4.518	5.14
36	90	Triangles	On edge	90	1.560	0.13

The tests were labeled according to the printing configurations, as indicated in Table 3.5.

Table 3.5: The codes of process parameters with results of warpage and deviation angles

Run	Codes	Warpage (mm)	Deviation angle (Degrees)
1	25LF45	2.175	0.99
2	25LF90	0.9755	0.24
3	25LO45	2.563	1.15
4	25LO90	1.452	2.12
5	25CF45	2.046	1.81
6	25CF90	1.062	1.71
7	25CO45	2.017	0.62
8	25CO90	1.882	4.42
9	25TF45	2.03	0.83
10	25TF90	0.9855	0.45
11	25TO45	1.79	0.49
12	25TO90	1.472	0.04
13	50LF45	1.576	1.45
14	50LF90	0.9142	0.8
15	50LO45	2.866	1.21
16	50LO90	1.663	2.42
17	50CF45	1.910	1.14
18	50CF90	1.136	1.75
19	50CO45	1.646	0.5
20	50CO90	1.511	0.47
21	50TF45	2.002	1.11
22	50TF90	0.9523	2.75
23	50TO45	3.312	1.56
24	50TO90	1.452	0.16
25	90LF45	1.641	1.66
26	90LF90	0.9094	0.49
27	90LO45	3.784	1.7
28	90LO90	1.634	0.74
29	90CF45	1.969	1.04
30	90CF90	0.9976	1.56
31	90CO45	1.850	0.43
32	90CO90	1.516	0.24
33	90TF45	1.652	1.38
34	90TF90	0.9304	1.28
35	90TO45	4.518	5.14
36	90TO90	1.56	0.13

The simulation results for the deviation angle are presented in Figure 3.5, comparing infill density of 25% with line infill pattern at raster angles of 45 and 90°, printed

both flat and on edge. Figure 3.6 depicts the simulation results for warpage, comparing a 50% infill density with a concentric infill pattern at raster angles of 45 and 90°, printed flat and on edge.

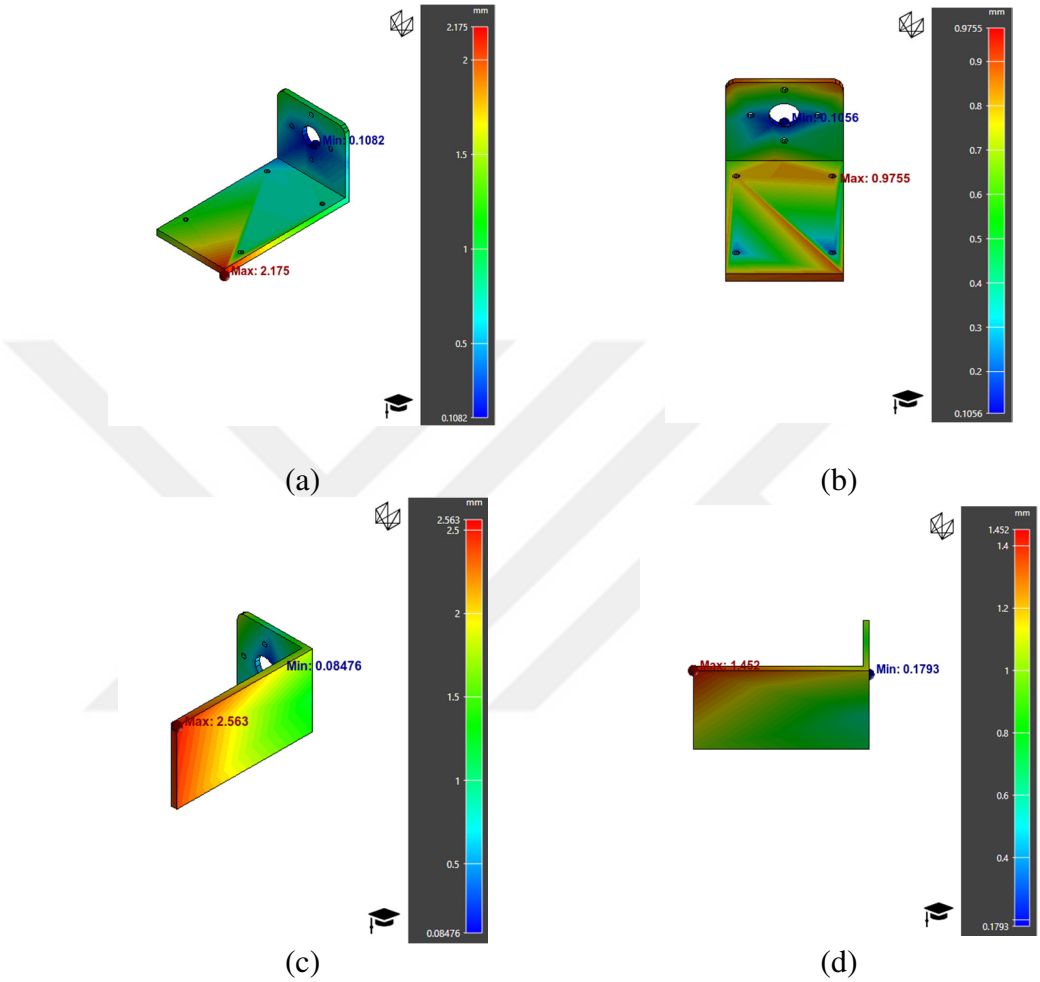

Figure 3.6: Results of warpage of infill density 25%, infill pattern lines: a) flat 45° b) flat 90° c) on edge 45° d) on edge 90°

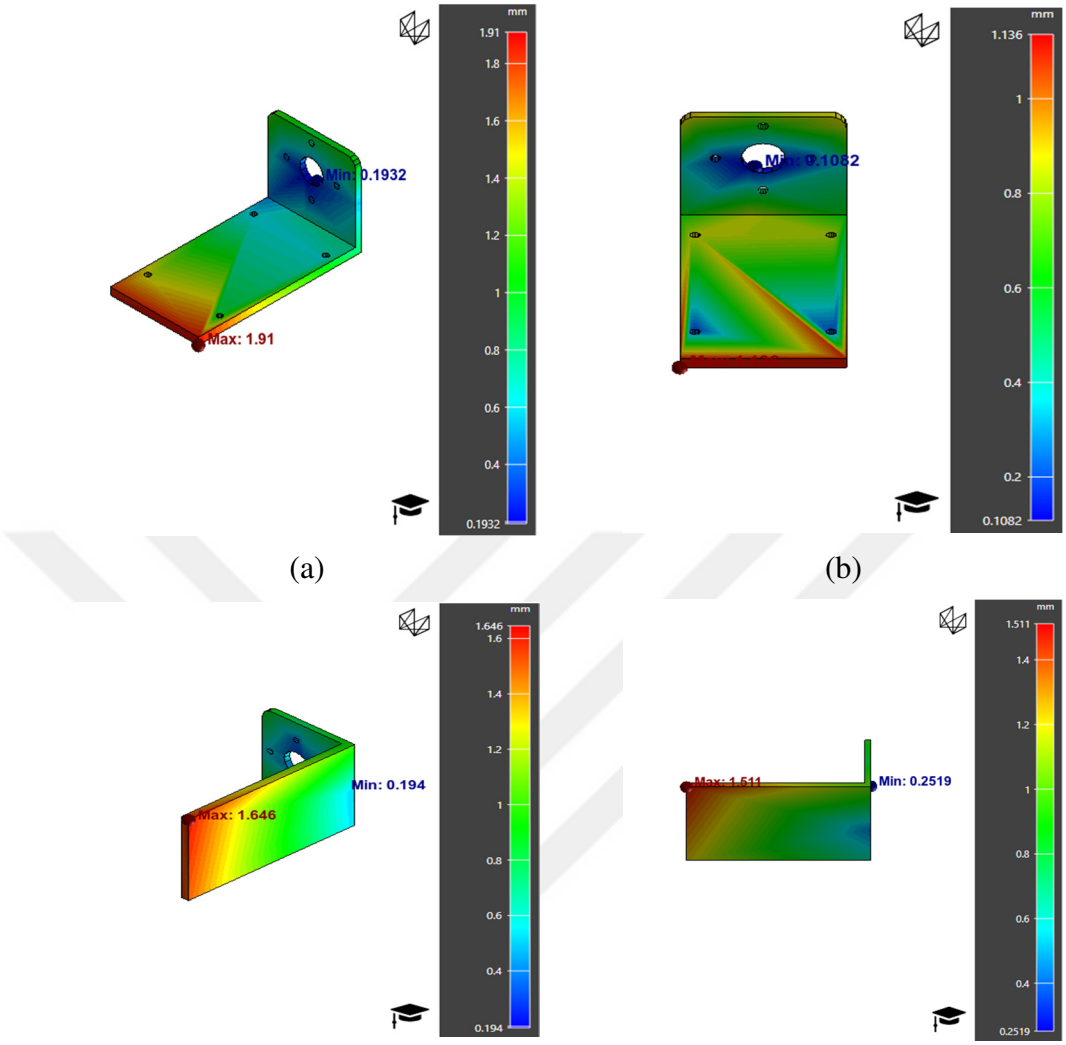

Figure 3.7: Results of warpage of infill density 50%, infill pattern is concentric: a) flat 45° b) flat 90° c) on edge 45° d) on edge 90°

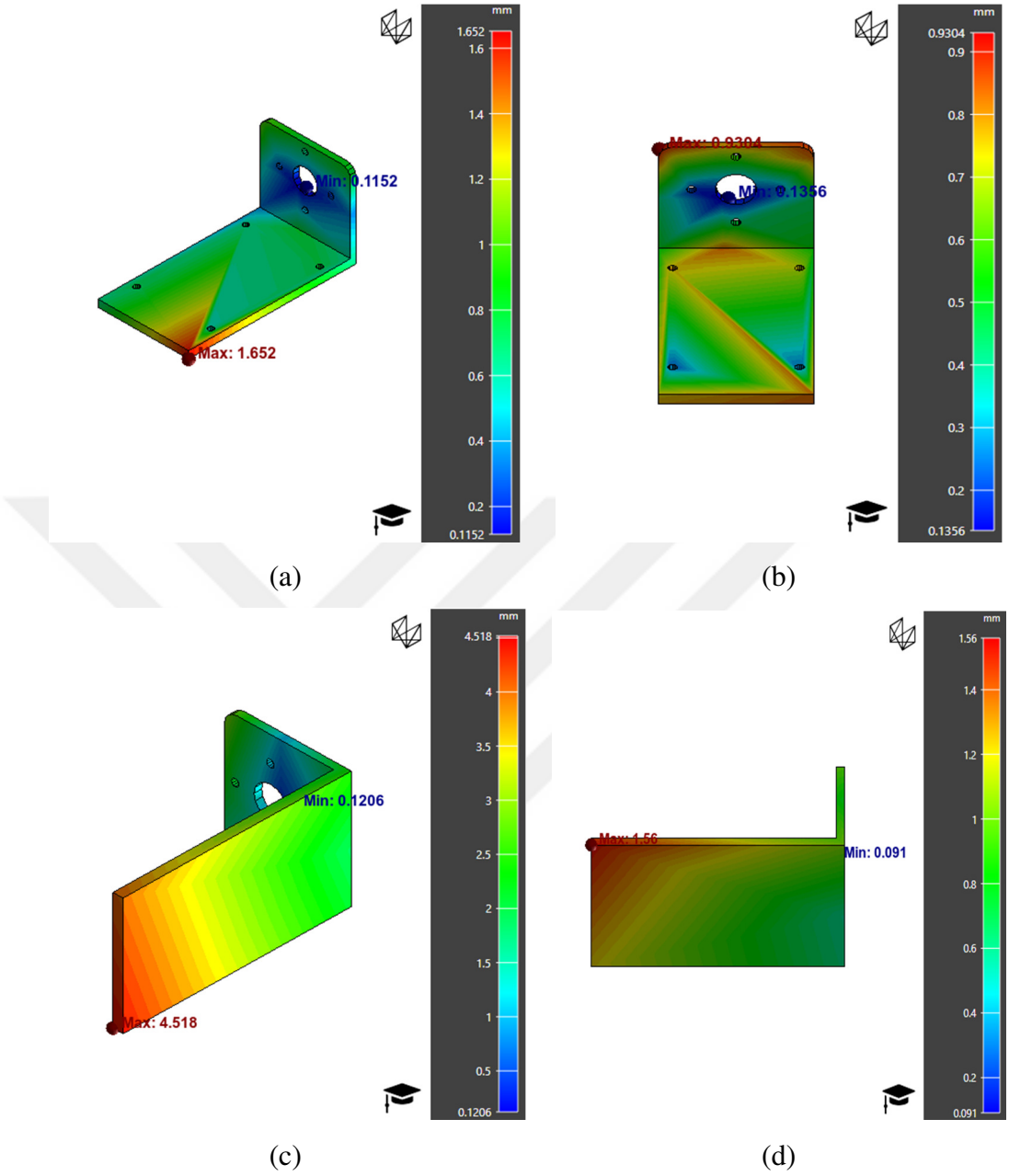

Figure 3.8: Results of warpage of infill density 90%, infill pattern is triangles: a) flat 45° b) flat 90°c) on edge 45° d) on edge 90°

Figure 3.8 represents the warpage results for an infill density of 90%, using a triangular infill pattern, printing in flat and on-edge directions, and raster angles of 45 and 90°.

The analysis of variance (ANOVA) was used to determine the effectiveness of the process parameters on the warpage and deviation angle. In ANOVA, the significance of each term is evaluated using Fisher's variance ratio (F-value) and probability value (P-value), which are calculated based on Degrees of freedom (DF), sequential sums of squares (Seq SS), adjusted sums of squares (Adj SS), the adjusted mean square (Adj MS). The P-value is probability against the null hypothesis, denoted as H0 and stated, "Treatment does not have a significant effect on response." Terms with p-values less than the significance level threshold ($\alpha = 0.05$) are considered significant terms. The analysis of variance on the warpage data in Table 3.5 is shown in Table 3.6.

Table 3.6: The analysis of Variance (ANOVA) for the Transformed Response for Warpage

Source	DF	Adj SS	Adj MS	F-Value	P-Value
Model	31	4.34329	0.14011	75.92	0.000
Linear	6	3.38668	0.56445	305.84	0.000
Infill density	2	0.00717	0.00358	1.94	0.258
Infill pattern	2	0.01242	0.00621	3.37	0.139
Printing direction	1	1.21350	1.21350	657.53	0.000
Raster angle	1	2.15358	2.15358	1166.90	0.000
2-Way Interactions	13	0.87675	0.06744	36.54	0.002
Infill density *infill pattern	4	0.01418	0.00354	1.92	0.271
Infill density * printing direction	2	0.04223	0.0211	11.44	0.022
Infill density * raster angle	2	0.00783	0.00391	2.12	0.236
Infill pattern * printing direction	2	0.09796	0.04898	26.54	0.005
Infill pattern * raster angle	2	0.07827	0.03913	21.20	0.007
Printing direction * raster angle	1	0.63630	0.63630	344.77	0.000
3-Way Interactions	12	0.07986	0.00666	3.61	0.113
Infill density * infill pattern * Printing direction	4	0.0555	0.01389	7.52	0.038
Infill density *infill pattern * Raster angle	4	0.00413	0.00207	1.12	0.411
Infill density * printing direction Raster angle	2	0.00054	0.00027	0.15	0.869
Errors	4	0.000738	0.00185		
Totals	35	4.35067			
Standard deviation (S) =0.0429599					
R^2=99.83%					
R^2_{adj}=98.52%					
R^2_{pred}=86.26%					

This study used the Box-Cox transformation to increase the models' anticipated accuracy and fit.

The response's metamorphosis can aid in addressing the problem of lack of fit. The experiment revealed that neither infill density nor infill design had a significant impact on the warpage's altered reactivity. The P-value is significantly more than 0.05 throughout 95% of the confidence interval, demonstrating this. However, the printing direction and raster angle have a significant impact on the warpage's modified reactivity.

Table 3.7: The analysis of Variance (ANOVA) for Transformed Response for Warpage after removing non-significant

Source	DF	Adj SS	Adj MS	F-Value	P-Value
Model	27	4.33862	0.16069	106.64	0.000
Linear	6	3.38668	0.56445	374.60	0.000
Infill density	2	0.00717	0.00358	2.38	0.155
Infill pattern	2	0.001242	0.00621	4.12	0.059
Printing direction	1	1.21350	1.21350	805.36	0.000
Raster angle	1	2.15358	2.15358	1429.26	0.000
2-Way Interactions	13	0.87675	0.06744	44.76	0.000
Infill density *infill pattern	4	0.01418	0.00354	2.35	0.141
Infill density * printing direction	2	0.04223	0.02111	14.01	0.002
Infill density * raster angle	2	0.00783	0.00391	2.60	0.135
Infill pattern * printing direction	2	0.09796	0.04898	32.51	0.000
Infill pattern * raster angle	2	0.07827	0.03913	25.97	0.000
Printing direction * raster angle	1	0.63630	0.63630	422.29	0.000
3-Way Interactions	8	0.07519	0.00940	6.24	0.009
Infill density * infill pattern * Printing direction	4	0.0555	0.01389	9.22	0.004
Infill density *infill pattern * Raster angle	4	0.0196	0.00491	3.26	0.073
Errors	8	0.01205	0.00151		
Totals	35	4.35067			
Standard deviation (S) =0.0388173					
R^2= 99.72%					
R^2_{adj}= 98.79%					
R^2_{pred}= 94.39%					

Table 3.7 shows the ANOVA results for Warpage's transformed response after removing non-significant terms. The infill density and pattern have no significant

effect on the warpage's transformed response since the p-value is greater than 0.05 in 95% of the confidence intervals.

However, the printing direction and raster angle have a major impact on the warpage's transformed reaction. After accounting for a variety of non-significant effects (errors), the estimated R-squared rose from 86.26% to 94.39%.

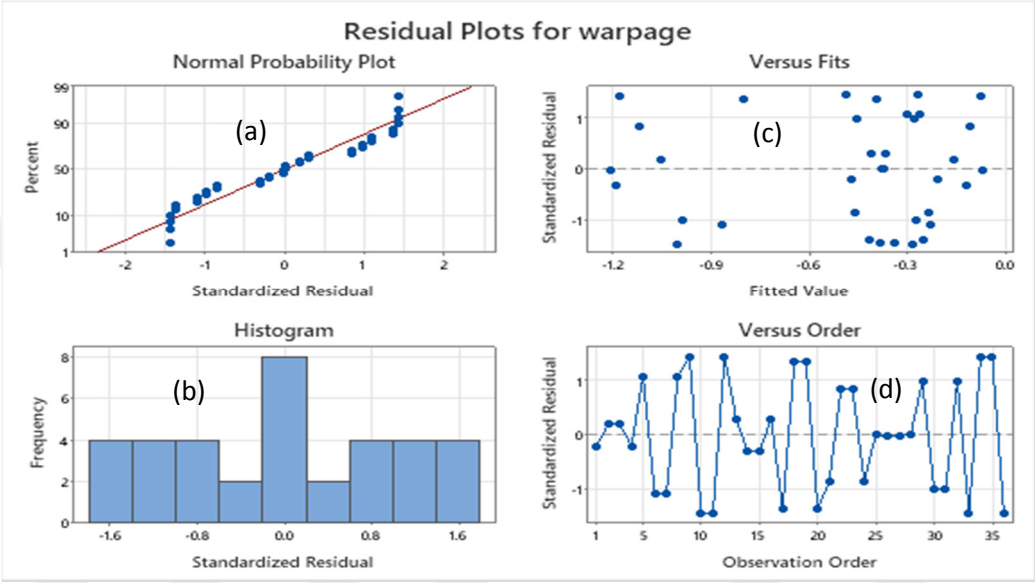

Figure 3.9: Residual plots for warpage: a) Normal probability plot b) Histogram c) Versus fits d) Versus order

Figure 3.9 depicts the residual plots, which provide a complete study of the residuals from a statistical model used to anticipate warpage in a fused deposition modeling (FDM) process. These plots are critical tools for diagnosing the model's behavior and testing the assumptions of normality, homoscedasticity, and residual independence, all of which are required for the model's findings to be true.

Figure 3.9 a) shows the normal Probability Plot assesses whether the model's residuals are normally distributed. The data points largely align with the red reference line, representing the expected distribution under normality. The close alignment suggests that the residuals approximate a normal distribution, validating one of the critical assumptions of linear regression. This normality assumption is supported by various statistical tests that rely on this property.

Figure 3.9 b) shows the histogram of Standardized Residuals plot visually represents the distribution of residuals. The histogram shows a relatively symmetrical distribution of residuals around zero, although it appears slightly skewed towards the right. The symmetry around zero generally supports the normality assumption, though the slight skewness might suggest minor deviations. However, these deviations do not appear severe enough to invalidate the model.

Figure 3.9 c) shows the residuals vs. Fitted Values Plot check for homoscedasticity (constant variance) of residuals across the range of fitted values. The plot displays a random scatter of residuals around zero without any apparent patterns or systematic structure. The absence of clear patterns, such as funnels or curves, suggests that the residuals have constant variance, affirming the model's homoscedasticity assumption. This indicates that the model's predictive accuracy does not vary at different levels of the fitted values.

Figure 3.9 d) shows the residuals vs. Order Plot and examines whether residuals are independent of each other, which is vital for the reliability of the regression model. The residuals show no apparent trends or cycles over time (or the order of data collection). This plot's lack of patterns or autocorrelation supports the assumption of independence among residuals. This implies that the residuals from one prediction do not influence those from another, an essential condition for the generalizability of the regression model.

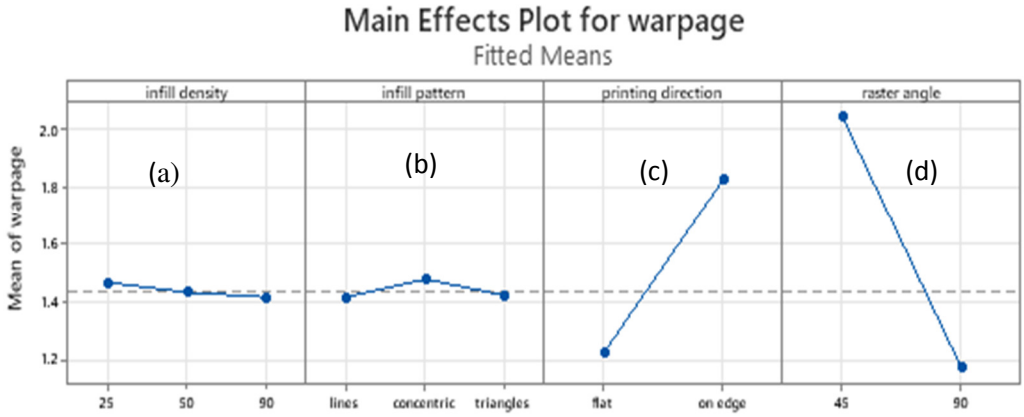

Figure 3.10: The main effects plots for warpage with respect to a) infill density (%), b) infill pattern, c) Printing orientation, d) Raster angle

The "Main Effects Plot for Warpage" (Figure 3.10) visualizes the impact of infill density, infill pattern, printing direction, and raster angle on the mean warpage observed in FDM.

Figure 3.10 a) depicts the Infill Density plot, which demonstrates that changes in infill density (25%, 50%, and 90%) have a generally constant and minor influence on warpage. The average warpage levels are essentially stable across densities, with just minor variations. This shows that infill density has no significant effect on warpage within the tested range. The material's response to different densities might be sufficiently uniform, suggesting that internal stresses due to density variations are not a significant contributor to warpage under these specific conditions.

Figure 3.10 b) shows the Infill Pattern appears consistent across different infill patterns: lines, concentric, and triangles. The similarity in warpage across these patterns indicates that the geometric configuration of the infill does not substantially affect the dimensional stability of the part. This could be attributed to the filament's material properties or the printed object's overall configuration, which may neutralize the impact of pattern variation.

Figure 3.10 c) shows the printing Direction was a notable difference in warpage between parts printed flat and those printed on edge. Printing flat results in significantly lower warpage compared to printing on edge. This was a critical finding as it highlights how the orientation of the print on the build platform can affect the cooling rates and stress distribution, thereby influencing warpage. Printing flat likely offers a more stable base and uniform cooling, reducing the development of internal stresses that lead to warpage.

Figure 3.10 d) shows the Raster Angle plot shows a dramatic decrease in warpage when the raster angle is changed from 45º to 90º. This indicates a strong dependence of warpage on the raster angle. A 90º raster angle may align more effectively with the principal stress directions in the print, thereby optimizing the layer adhesion and

stress distribution across the print. This alignment could significantly mitigate the internal stresses that cause warpage.

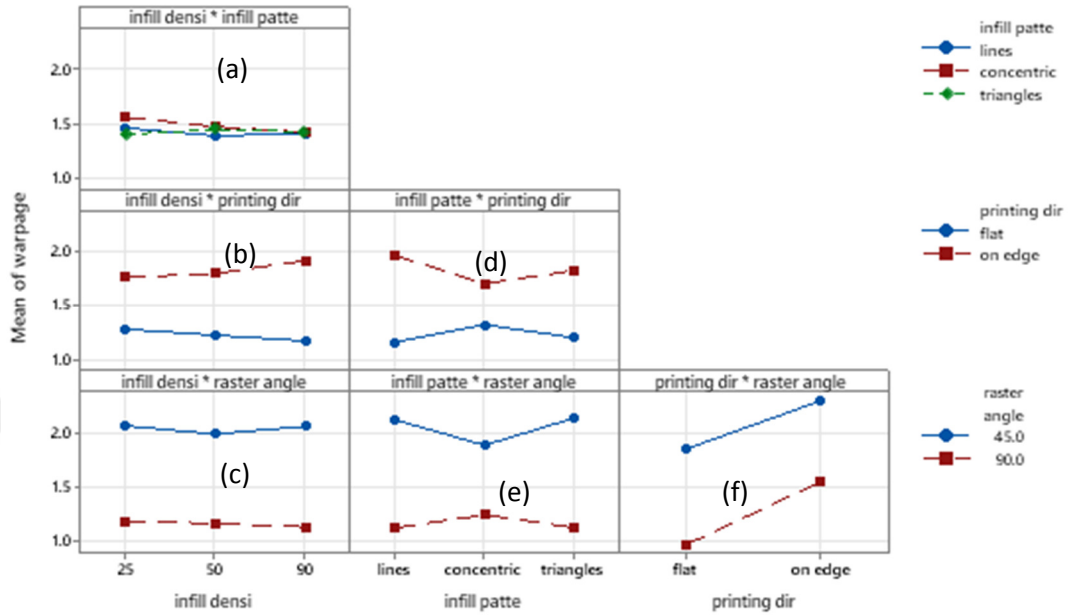

Figure 3.11: Results of interaction plots for warpage: a) infill density, infill pattern b) infill density, printing orientation c) infill density, raster angle d) infill pattern, printing orientation e) infill pattern, raster angle f) printing orientation, and raster angle.

Interaction plots were used to identify whether the effect of one factor on the warpage depends on the level of another factor.

Figure 3.11 a) illustrates the relationship between infill density and infill pattern, where infill density is plotted against the warpage. This figure shows that changes in infill density do not affect the infill pattern, as all interactions exhibit a warpage of 1.5mm, which does not demonstrate a significant effect. The interaction plot between infill density and infill pattern for warpage would reveal whether specific infill patterns are more effective at minimizing warpage at certain densities. When non-parallel lines are indicated, a significant interaction is suggested, implying that the optimal infill pattern for reducing warpage varies with infill density.

Figure 3.11 b) Infill density, printing orientation: A significant effect is shown by infill density because all of them are in lines. Printing direction includes flat and on

edge. For these two printing directions, the one with a low warpage, flat, has been selected as compared to the one on the edge, which exhibits a high warpage.

This interaction plot is used to examine how the effect of infill density on the warpage varies with different printing directions. Non-parallel lines indicate that certain printing directions are better suited to specific infill densities for minimizing warpage. For instance, higher infill densities are associated with on-edge printing, which is why flat printing, which exhibits less warpage than on-edge printing, has been chosen. Directional dependency on the optimal infill density for reducing warpage is indicated by flat printing.

Figure 3.11 c) shows two raster angles: 45 and 90 degrees. A significant effect is demonstrated by infill density; however, better results are given by 90°, as it is associated with lower warpage. An interaction plot for infill density and raster angle can be used to reveal how the warpage is affected by changes in the raster angle at different infill densities. Non-parallel lines in the plot indicate that the impact of raster angle on the warpage varies with infill density. Warpage is minimized specifically by a raster angle of 90°.

Figure 3.11 d) presents two printing directions: flat and on edge. The infill pattern demonstrates a significant effect. Better results are provided by printing flat instead of on edge due to its lower warpage. This interaction plot would aid in understanding whether specific infill patterns are more susceptible to warpage when printed in specific directions. An interaction is indicated by non-parallel lines in the plot, meaning that an infill pattern's effectiveness in reducing warpage depends on the printing direction. Warpage may be better minimized by some patterns when printed flat rather than on edge.

Figure 3.11 e) Infill pattern, Raster angle: A significant effect is shown by the infill pattern; however, as the infill pattern includes 45 degrees and 90 degrees, 90° has been selected, which shows better results. This plot can identify combinations that minimize warpage by analyzing the interaction between the infill pattern and raster

angle. Intersecting or non-parallel lines suggest that the best infill pattern for reducing warpage is changed to a raster angle of 90°.

Figure 3.11 f) Printing orientation, Raster angle: The raster angle consists of 45 and 90°. The printing orientation has a significant effect, and here, we prefer 90° as it has a low warpage. This plot explores how the combination of printing direction and raster angle influences warpage. A significant interaction, shown by non-parallel lines, would indicate that the effect of the raster angle on the warpage depends on the printing direction. Certain angles may effectively reduce warpage when printing in one direction but not in another, 90° will give better results. Suggesting a need to consider both factors when optimizing print settings to minimize warpage.

Table 3.8 displays the analysis of variance (ANOVA) of the transformed response for deviation angle. infill density has no significant effect on the transformed response for deviation angle, since the P-value is substantially bigger than 0.05 for 95% confidence interval. However, infill pattern, printing direction, and raster angle all have a considerable impact on the converted response to deviation angle.

Table 3.8: The analysis of Variance (ANOVA) for the transformed response of deviation angle

Source	DF	Adj SS	Adj MS	F-Value	P-Value
Model	31	34.4413	1.11101	17.98	0.006
Linear	6	5.9211	0.98685	15.97	0.009
Infill density	2	0.5159	0.25794	4.17	0.105
Infill pattern	2	1.5358	0.76791	12.43	0.019
Printing direction	1	1.6678	1.66776	26.99	0.007
Raster angle	1	2.2016	2.20163	35.63	0.004
2-Way Interactions	13	17.5536	1.35028	21.85	0.004
Infill density *infill pattern	4	5.9296	1.48241	23.99	0.005
Infill density *printing direction	2	0.4317	0.21585	3.49	0.133
Infill density *raster angle	2	1.1873	0.59366	9.61	0.030
Infill pattern *printing direction	2	5.0017	2.50086	40.47	0.002
Infill pattern *raster angle	2	4.4573	2.22867	36.06	0.003
Printing direction *raster angle	1	0.5459	0.54587	8.83	0.041
3-Way Interactions					
Infill density *infill pattern *	12	10.9666	0.91389	14.79	0.009

Printing direction Infill density *infill pattern * Raster angle	4	1.5362	0.38404	6.21	0.052
Infill density *printing direction * Raster angle	4	0.7415	0.18536	3.00	0.156
Infill pattern *printing direction *Raster angle	2	0.2472	3.45047	55.83	0.001
Errors	4	34.6885	0.06180		
Totals	35				

Figure 3.12 shows the residual plots for deviation angle with respect to the normal probability plots, histogram, versus fits, and order.

Analyzing residual plots in Minitab for the deviation angle in a statistical model provides critical insights into the model's assumptions and performance.

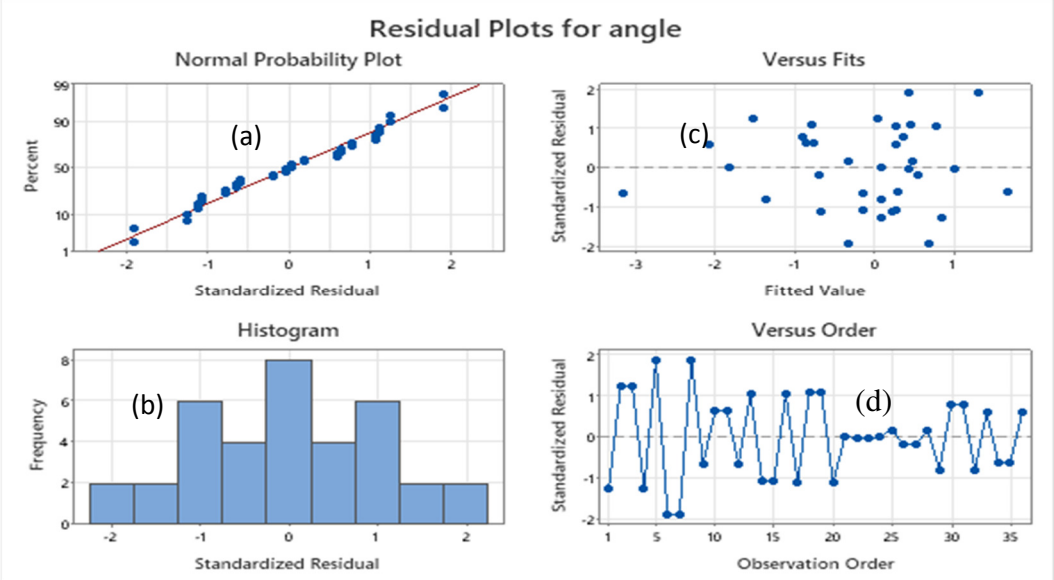

Figure 3.12: The residual plots of deviation angle: (a) Normal probability plot (b) Histogram (c) Versus Fits (d) Versus order

Figure 3.12 a) represents the normal Probability PlotThe data points closely follow the red diagonal line, representing the expected distribution under the normality assumption.

Figure 3.12 b) shows the histogram of Standardized Residuals, The histogram displays a roughly bell-shaped distribution but shows some potential skewness or excess kurtosis, as indicated by the slight asymmetry and peakedness. While the histogram supports the indication of normality to some extent,

The visible skewness and peakedness could suggest deviations that might affect the robustness of the regression model's estimations. This warrants further investigation or potentially the use of robust statistical methods.

Figure 3.12 c) shows the residuals vs. Fitted Values, The plot shows residuals scattered randomly around the horizontal axis without any apparent pattern. The lack of a discernible pattern or systematic form (e.g., funnel shape) suggests that the residuals have constant variance, affirming the homoscedasticity assumption. This randomness is crucial for ensuring that the model provides unbiased and consistent predictions across all values of the independent variables.

Figure 3.12 d) shows the residuals vs. Order Plot and examines whether residuals are independent of the order in which data are collected or modeled, checking for autocorrelation. The residuals appear randomly distributed without any obvious trends or cyclic patterns. The randomness observed in this plot indicates that there is no autocorrelation present among the residuals. This supports the assumption that each residual is independent of the others, an essential requirement for many forms of regression analysis.

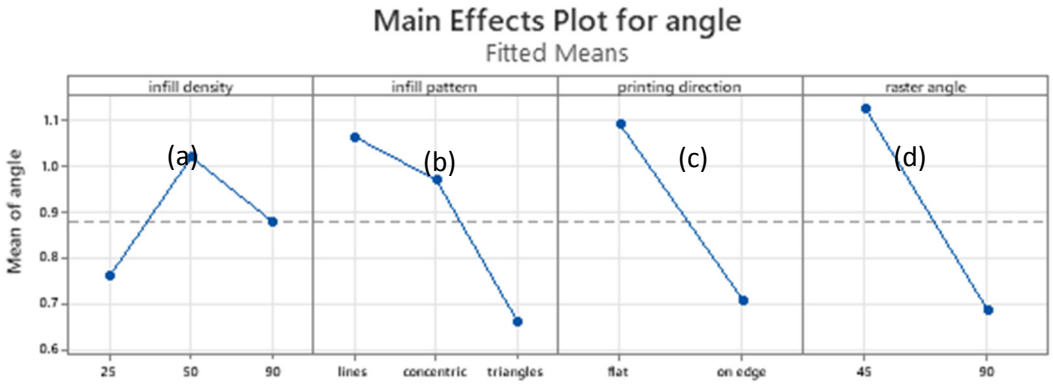

Figure 3.13: The main Effects plots for deviation angle concerning a) infill density, b) infill pattern, c) printing direction, d) raster angle

The Main Effects Plot for the deviation angle in Figure 3.13 shows:

Figure 3.13 a) the main effects plot for infill density may reveal a trend in which increasing or decreasing density influences the deviation angle. A lower deviation angle is preferable, indicating a better fit to the desired design. If the plot shows that higher infill densities result in lesser deviation angles, this indicates that a denser structure provides better support and stability for the L-shape, reducing distortion. Conversely, if lower densities enhance accuracy, less internal tension during cooling aids in maintaining the intended tilt. We used a 25% infill density, which results in a modest deviation angle.

Figure 3.13 b) we have different infill patterns (like lines, concentric, and triangles). Still, triangles influence the internal structure's stability and how it supports the L-shape, thereby giving a low deviation angle. The main effects plot can reveal which patterns are more conducive to maintaining accurate angles. We have selected triangles with low deviation angles that can offer more uniform support across different orientations.

Figure 3.13 c) Printing direction can significantly affect the accuracy of printed angles due to the way layers are deposited and how gravity impacts the part during printing. The main effects plot for printing direction will indicate if specific orientations (e.g., printing the L-shape flat vs. on edge) lead to better alignment between the camera holder and the camera itself. The on-edge direction will minimize the deviation angle, which would be ideal, suggesting it offers better structural integrity and alignment during printing.

Figure 3.13 d) shows that the raster angle, or the orientation of the print lines within each layer, can affect how forces are distributed within the material, potentially impacting the deviation angle of the L-shape. The main effects plot for the raster angle might show specific angles that result in closer adherence, such as 90 degrees. Optimal raster angles will minimize the deviation, indicating that the internal stresses and layer adhesion are conducive to maintaining the shape's accuracy.

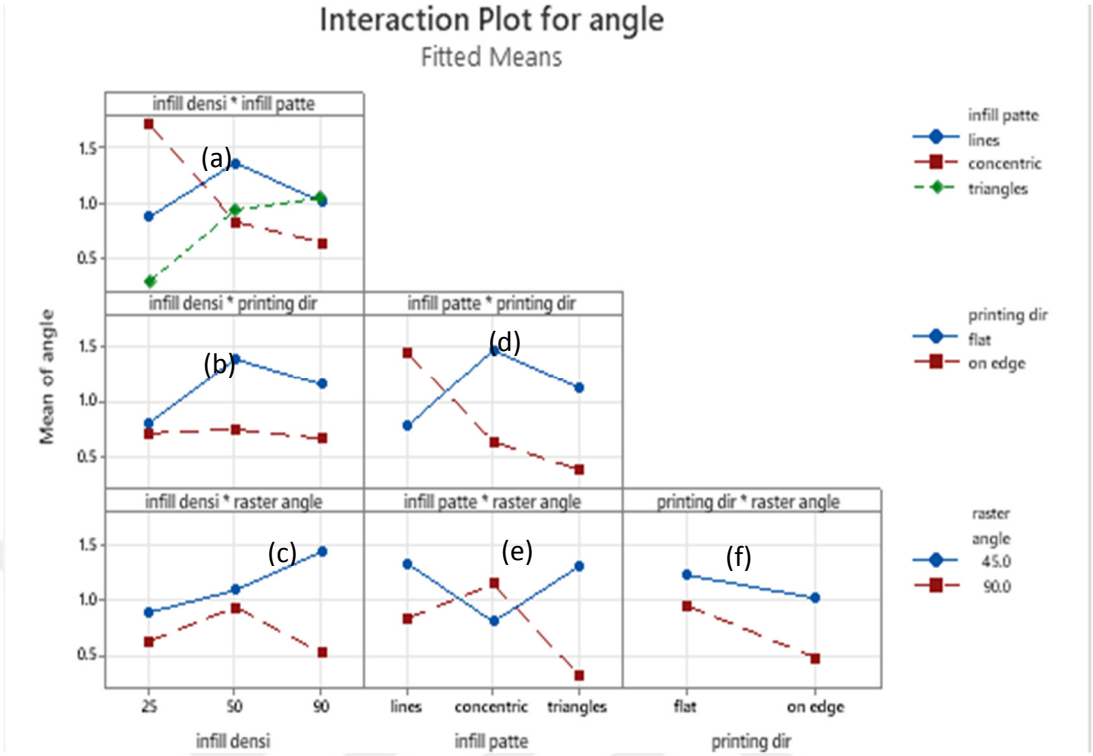

Figure 3.14: The interaction plot for deviation angle with respect to a) infill density, infill pattern b) infill density, printing direction c) infill density, raster angle d) infill pattern, printing direction e) infill pattern, raster angle f) printing direction, and raster angle

Figure 3.14, generally provides an analysis of the interaction plots between various FDM printing parameters and their impact on the printing process's outcome.

Figure 3.14 a) Infill Density & Infill Pattern, This plot shows that as infill density increases from 25% to 50%, the deviation angle tends to decrease, particularly for the lines and concentric patterns. However, further increase to 90% infill density increases deviation for lines, while it decreases for triangles. The varying trends suggest that the effectiveness of an infill pattern in controlling deviation is highly dependent on the density of the infill. Triangles may provide more stability at higher densities, likely due to better distribution of internal stresses.

Figure 3.14 b) Infill Density & Printing Direction, Printing on edge consistently results in lower deviation angles across all infill densities than printing flat. The orientation of the part during printing significantly affects the outcome.

Printing on edge minimizes deviation by providing a more stable base during the printing process, further enhanced by increased infill.

Figure 3.14 c) Infill Density & Raster Angle, A raster angle of 90° consistently results in lower deviation angles, which is more pronounced at higher infill densities. A raster angle of 90° likely aligns better with the load directions during printing, thereby reducing the likelihood of warpage and resulting deviation. The effectiveness of this alignment increases with infill density.

Figure 3.14 d) Infill Pattern & Printing Direction: Printing on the edge generally results in lower deviation angles for all infill patterns, with concentric patterns exhibiting the least impact on deviation when printed on the edge. The infill pattern's directional dependency highlights how gravity and layer adhesion interact differently based on printing orientation. Concentric patterns might provide more consistent layer adhesion across changes in orientation.

Figure 3.14 e) Infill Pattern & Raster Angle, The triangular pattern combined with a 90° raster angle shows the least deviation, particularly when compared to lines and concentric patterns at a 45°. The triangular pattern possibly offers better internal structure to counteract the forces during printing that lead to warpage, especially when aligned with a raster angle that complements the geometry of the pattern.

Figure 3.14 f) Printing Direction & Raster Angle, The combination of printing flat with a 90° raster angle results in the lowest deviation angles, indicating optimal alignment and support during printing. This result underscores the importance of aligning raster angles with the primary dimension of the part to optimize structural integrity and minimize stress concentration.

3.8 Response Optimization of Warpage and Deviation Angle

The optimization study focused on minimizing two critical parameters: warpage and deviation angle. Such parameters are crucial in manufacturing contexts, particularly in precision engineering and additive manufacturing, where dimensional accuracy and alignment are key. Process parameters and material compositions have been adjusted systematically to minimize warpage in FDM printed composites. This optimization ensures that the final printed parts meet dimensional accuracy and quality standards.

Table 3.9: Response optimization

Response	Goal	Lower	Upper
Warpage	Minimize	0.9094	4.518
Deviation angle	Minimize	0.04	5.14

Table 3.10: The solution of response optimization

Solution	Infill density	Infill pattern	Printing direction	Raster angle	Warpage (Fit)	Deviation angle (Fit)	Composite Desirability
1	25%	Triangle	Flat	90°	0.998	0.317	0.960

Based on Tables 3.9 and 3.10, the main objective of response optimization was to find optimal settings for multiple input variables based on desired outcomes for output variables and to reduce the warpage and deviation angle response. The suitable infill density was 25%, and the infill pattern was set to triangles. The printing direction was flat, and the raster angle was 90º. The results showed that the warpage was reduced to 0.91mm, and the minimum deviation angle was 0.04º.

3.9 Conclusion

Considering the presented results in this chapter, it can be concluded that:

- Infill Density: Set at 90%, this high density helps ensure the part has sufficient internal support, effectively minimizing the internal stresses leading to warpage during the cooling phase.
- Infill Pattern: A-line pattern was selected. This pattern provides a consistent and uniform internal structure, which aids in maintaining dimensional stability throughout the printing process.
- Printing Direction: The parts were printed in a flat orientation. This orientation is advantageous because it allows for a more even heat distribution during printing and cooling, which is crucial for reducing thermal stress.
- Raster Angle: The raster orientation was chosen at a 90°. This angle helps balance the material deposition, optimizing the part's strength and reducing the likelihood of warping due to uneven material layering.

  These parameters were carefully selected to overcome the warpage problem in FDM printing. Balancing and fine-tuning these settings improved the printing process's stability and enhanced the final product's quality. The optimized settings have delivered superior results and proven a practical approach to addressing one of the most persistent challenges in FDM printing.

- Infill Density: An infill density of 25% was optimal. This lower density likely facilitates faster cooling and solidification, reducing internal stresses that can cause deformation and, thus, angular deviation.
- Infill Pattern: The triangle pattern was selected for its structural benefits. Triangle patterns can provide excellent stability and even stress distribution within the part, which contributes to maintaining the intended angles during printing.
- Printing Direction: Printing 'on edge' was determined to be the most beneficial. This orientation may help align the part more stably on the print bed, ensuring the layers build up to minimize shifts or distortions.

- Raster Angle: A 90° was chosen. Aligning the material deposition perpendicular to the primary load or stress direction can help optimize the mechanical properties, particularly rigidity and dimensional stability, thereby reducing the likelihood of deviation.

CHAPTER 4

EXPERIMENTAL ANALYSIS OF MECHANICAL PROPERTIES

4.1 Sample Preparation

The samples were printed with Raise3D Industrial PA12-CF carbon fiber-reinforced composite filament based on Polyamide 612 (Nylon 612). This filament contains 15% carbon fiber and has a perfect length distribution. The major purpose of this experiment was to investigate how infill density (25%, 50%, 90%), infill design (lines, concentric, triangles), and raster angle (45° and 90°) affected the mechanical qualities of 3D printed PA12CF15.

Table 4.1: The process parameters and their levels

Run	Process parameters	Levels
1	Infill density (%)	25%, 50%, 90%
2	Infill pattern	Lines, Concentric, Triangles
3	Raster angle	45º, 90º

To analyze the impact of each variable, we have systematically varying three selected process parameters across a series of 18 specimens in a controlled environment. Tensile test samples were printed according to ASTM D638 using the RAISE3D E2CF printer (Figure 4.1).

Figure 4.1: Fabricated tensile test samples

4.2 Tensile Test

The 3D-printed specimens have a cross-section of 13.4 mm width and 3.7 mm thickness at the gauge length.

Figure 4.2: The schematic of tensile testing equipment

When the breaking point is observed at an infill density of 25% in the middle of the printed part, the infill density is increased to 50%, and it is observed that the breaking occurs below the middle. This indicates that the breaking point occurs below the center when the infill density is increased.

The breaking point and ultimate tensile strength (UTS) on the lines or rectilinear infill pattern tends to exhibit a directional dependence on mechanical strength. The breaking point for materials with this pattern is typically lower than for more complex patterns, owing to the alignment of material deposition in a single direction. This configuration may lead to easy propagation of cracks along the lines, leading to a lower UTS. Stiffness in parts with a line pattern is also directionally dependent. While the material might exhibit higher stiffness along the lines due to continuous

filament paths, perpendicular forces can easily compromise this stiffness, leading to early deformation.

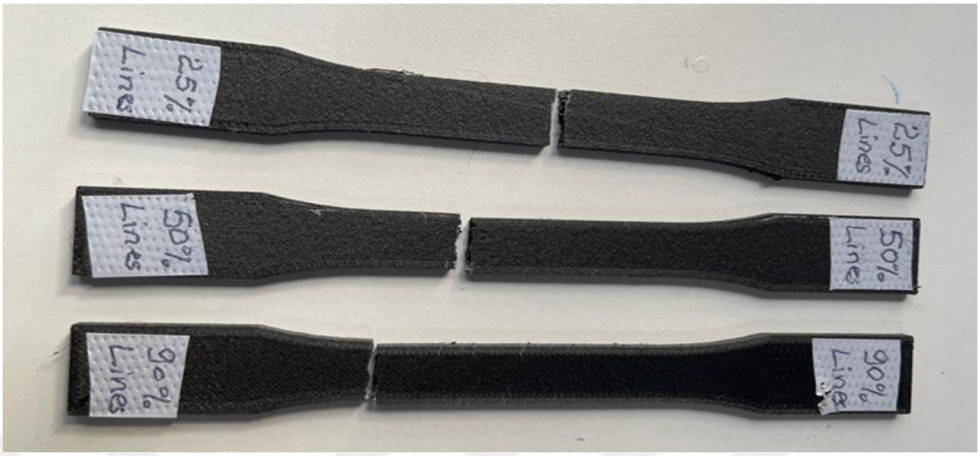

Figure 4.3: The sample of the infill pattern is Lines with different infill densities: a) 25%, b) 50%, and c) 90% after the breaking point

When the breaking point is observed at an infill density of 25% in the middle of the printed part, the infill density is increased to 50%, and the breaking is then observed to occur below the middle. This means the breaking point happens below the center when we increase the infill density. The breaking point on the ultimate tensile strength (UTS) on the concentric infill patterns, which follow the perimeter of the part, provides improved load distribution around the part's edges. This pattern tends to increase the breaking point and UTS for parts subjected to evenly distributed loads or symmetrical stresses.

The uniform distribution of material can resist crack propagation better than the line pattern, leading to a higher UTS. The concentric pattern also enhances stiffness, particularly in parts with circular or complex outer geometries. The continuous path of material around the shape helps maintain structural integrity under load, providing a uniform response to stress and reducing the likelihood of localized deformation. When examining how concentric infill patterns with varying densities from 25% to 90% affect the fracture behavior of a 3D printed part during a tensile test, several key points emerge:

The portion has a modest infill density (25%), resulting in greater flexibility and less density. This leads to lower mechanical characteristics, making the part more prone to deformation and failure under tensile stress. The reduced amount of material in the construction causes inferior stress distribution.

As a result, the fracture is more likely to occur at the grip zones, where clamping causes the most stress concentration. The image below illustrates that the material cannot effectively hold the load, resulting in early failure. As seen in Figure 4.4.

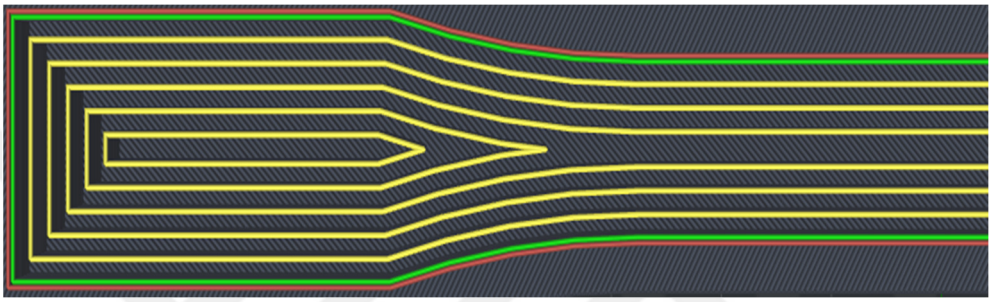

(a)

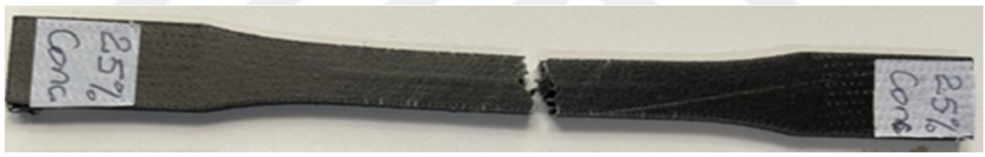

(b)

Figure 4.4: Presentation of (a) grip zone from Ideamaker and (b) fracture point with infill density of 25%

On the other hand, a medium infill density of 50% offers a promising balance between strength and flexibility. The part gains more mechanical strength and rigidity compared to 25% infill, while still retaining a degree of flexibility.

This equilibrium allows for better stress distribution across the part. Although the fracture may still occur below the grip zones, the likelihood is significantly reduced compared to 25% infill. The greater amount of material allows for more effective stress absorption and distribution. However, at heavy loads, the weakest places near the grips may fail first. As illustrated in Figure 4.5.

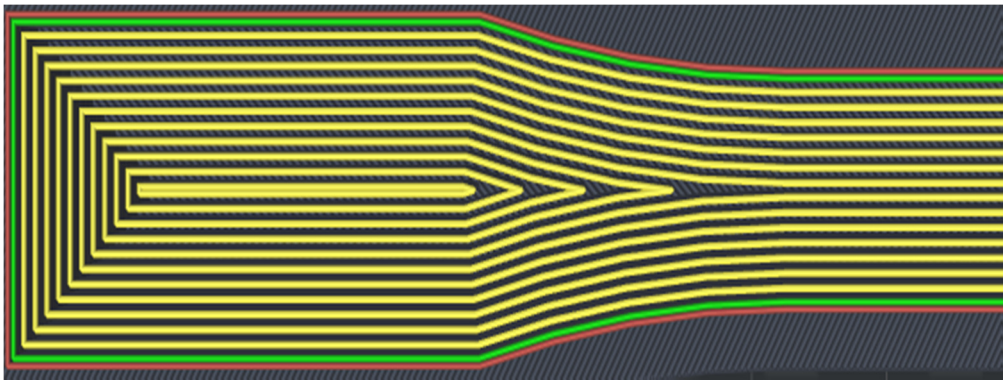

(a)

(b)

Figure 4.5: Presentation of (a) grip zone from Ideamaker (b) fracture point with infill density of 50%

When a part is printed with a High % Infill Density of 90%, it is almost solid, making it incredibly strong and rigid. This infill density is suitable for applications that require robust mechanical properties. The material's capacity to distribute stress has substantially increased, lowering the fracture risk at the grip zones. However, if substantial misalignment or insufficient clamping pressure occurs, fractures are more likely to occur away from the grips, where uniform tensile stress is exerted. As indicated in Figure 4.6.

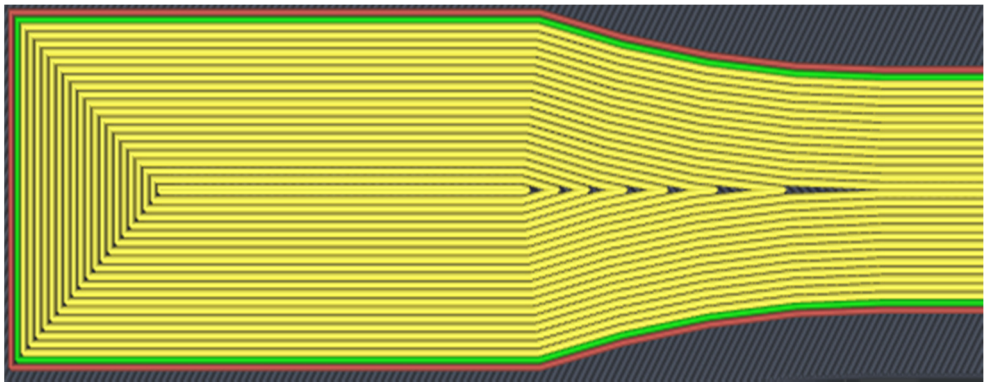

(a)

(b)

Figure 4.6: presentation of (a) grip zone from Ideamaker (b) fracture point with infill density of 90%

Fractures that occur close to the grip zone during tensile tests, such as those in ASTM D638, can be due to several factors primarily related to the setup and handling of the specimen during the test. One of the main reasons is specimen misalignment. If the specimen is not held perpendicular to the jaw faces, it can lead to uneven stress distribution, causing the material to fail near the grips where stress concentrations are highest. Proper alignment is crucial; using alignment devices can help ensure the specimen is correctly positioned in the testing machine.

The triangle infill pattern's breaking point and ultimate tensile strength (UTS) are renowned for their mechanical efficiency. It offers the highest breaking point and UTS among the three patterns. Triangles' geometric stability, capable of distributing loads evenly across all directions, significantly hampers the initiation and propagation of cracks. This pattern effectively utilizes material properties to bear tensile loads, delaying failure and increasing the UTS. On the side of stiffness, the

triangular pattern outperforms its counterparts due to its ability to maintain structural integrity and resist deformation under various loading conditions.

The interconnected triangular structures create a robust internal framework that significantly enhances the material's response to stress, offering superior stiffness.

4.3 Design of Experiment Analysis Using Response Surface Methodology

The effect of process parameters on printed PA12CF was investigated statistically using response surface methods. MINITAB 21.1.0 was the program utilized in the analysis.

Table 4.2: The process parameters

No	Process parameters	Levels and values
1	Infill density (%)	25%, 50%, 90%
2	Infill pattern	Lines, Concentric, Triangles
3	Raster angle (Degrees)	45º, 90º

Table 4.2 displays the infill density at various percentages: 25%, 50%, and 90%. Furthermore, in the Infill Pattern—consisting of lines, triangles, and concentric circles—the raster angle is adjusted to 45º and 90º degrees to ascertain the effect of print layer orientation on the mechanical properties.

4.4 The Results of Ultimate Tensile Strength

Table 4.3 presents tensile test results, showing the results of ultimate tensile strength (UTS) and stiffness with raster angles of 45° and 90°.

Table 4.3: The results of Ultimate tensile strength and stiffness with a raster angle of 45º and 90°

No	Sample ID	Infill density (%)	Infill pattern	Raster angle	UTS (Mpa)	Stiffness (Gpa)
1	25-Line-1	25	Lines	45º	24.8	1.3
2	50-Line-1	50	Lines	45º	27.3	1.32
3	90-Line-1	90	Lines	45º	37.9	1.36
4	25-Line-2	25	Lines	90º	28.9	1.6
5	50-Line-2	50	Lines	90º	34.2	1.9
6	90-Line-2	90	Lines	90º	44.4	2.03
7	25-Concentric-1	25	Concentric	45º	12.81	1.25
8	50-Concentric-1	50	Concentric	45º	25.57	1.4
9	90-Concentric-1	90	Concentric	45º	44.13	2.15
10	25-Concentric-2	25	Concentric	90º	21.52	1.4
11	50-Concentric-2	50	Concentric	90º	30.07	1.86
12	90-Concentric-2	90	Concentric	90º	45.58	2.57
13	25-Triangle-1	25	Triangles	45º	24.3	1.08
14	50-Triangle-1	50	Triangles	45º	29.7	1.1
15	90-Triangle-1	90	Triangles	45º	36.5	1.8
16	25-Triangle-1	25	Triangles	90º	30.2	1.67
17	50-Triangle-2	50	Triangles	90º	33.2	1.76
18	90-Triangle-2	90	Triangles	90º	39.1	1.86

Table 4.3 shows the results of the ultimate tensile strength (UTS) and stiffness for various infill densities, patterns, and raster angles, demonstrating significant variability influenced by these parameters.

On the side of ultimate tensile strength:

UTS generally increases with higher infill densities. Samples with 90% infill exhibit the highest UTS across all patterns and raster angles. For instance, the 90% infill with lines pattern and 45º raster angle shows a UTS of 37.9 MPa, while the 25% infill shows a much lower UTS of 24.8 MPa. The concentric pattern at 90% infill with a 90º raster angle demonstrates the highest UTS of 45.58 MPa among the infill patterns. A raster angle 90º tends to enhance the UTS compared to 45º, especially noticeable in the higher infill densities. For example, at 90% infill, the line pattern with a 90º raster angle achieves a UTS of 44.4 MPa, higher than the 45º raster angle counterpart with 37.9 MPa.

On the side of stiffness:

Stiffness increases with infill density. The highest stiffness value is observed in the 90% infill concentric pattern with a 90º raster angle, reaching 2.57Gpa. Lower infill densities, such as 25%, show significantly lower stiffness. For example, the 25% infill lines pattern with a 45º raster angle has a stiffness of 1.3Gpa. Concentric patterns at higher infill densities are stiffer than lines and triangles. Sample 12 (90% infill, concentric, 90º raster angle) has the highest stiffness of 2.5Gpa.

A 90º raster angle yields higher stiffness values than a 45º raster angle. For instance, at 90% infill, the line pattern with a 90º raster angle (Sample 6) has a stiffness of 2.03Gpa, compared to the 45º raster angle counterpart (Sample 3), which has 1.36Gpa.

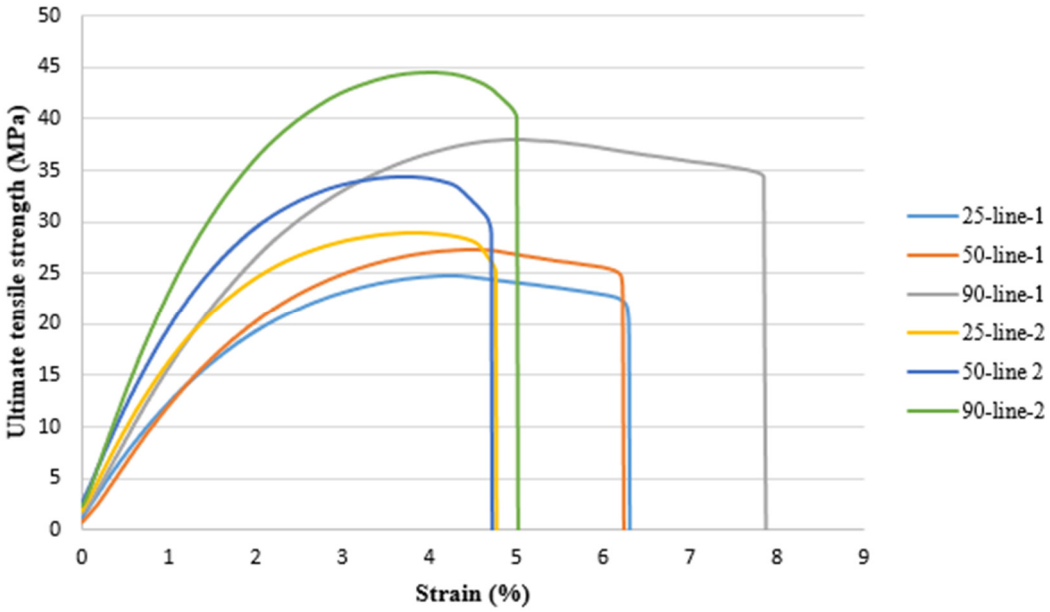

Figure 4.7: The results of ultimate tensile strength with different infill densities a) 25% b) 50% c) 90%, lines as infill pattern with raster angle of 45 and 90°

Figure 4.7 presents the stress vs strain diagram for the presented samples in Table 4.3. UTS values increase from 24.8 MPa at 25% density to 27.3 MPa at 50% density, reaching 37.9 MPa at 90%. This progression indicates a notable improvement in strength

as the material becomes denser, although the increase is gradual between 25% and 50% and more pronounced between 50% and 90%. Also, for (90° raster angle), UTS values start higher at 28.9 MPa for 25% density, move to 34.2 MPa at 50% density, and peak at 44.4 MPa for 90% density. The improvement in strength is consistent across densities, with the change in raster angle contributing to the higher UTS values compared to the 45-degree angle at all levels of infill density.

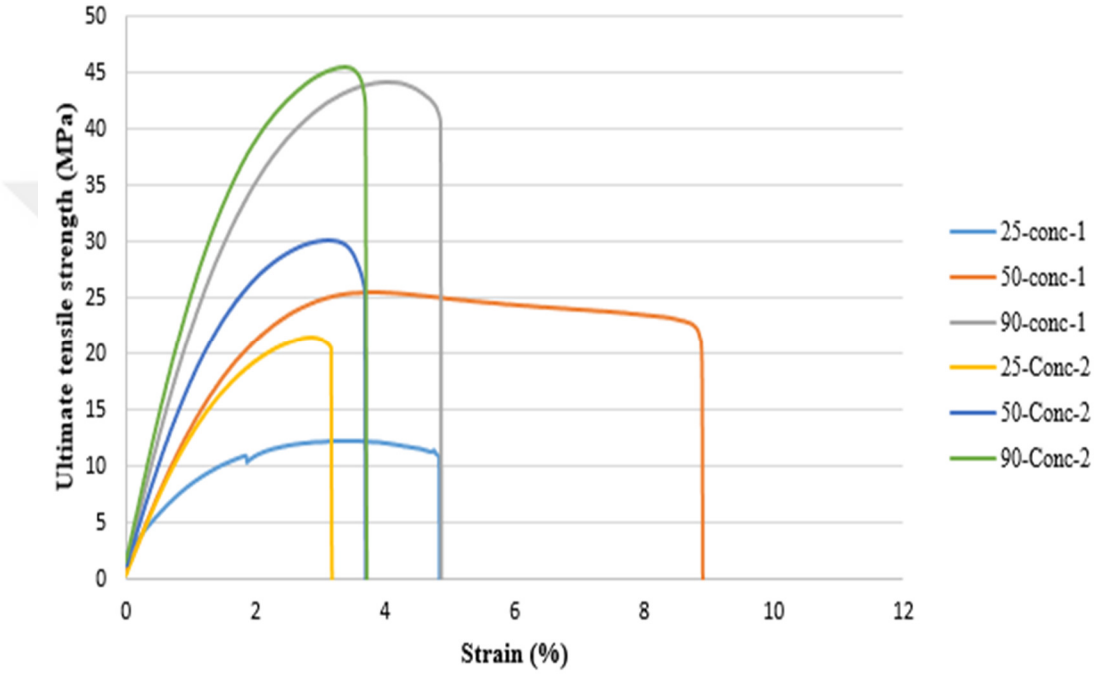

Figure 4.8: The results of ultimate tensile strength with different infill densities a) 25% b) 50% c) 90%, concentric as infill pattern with raster angle of 45 and 90°

Figure 4.8 displays the ultimate tensile strength of 3D printed samples with varying infill densities using a concentric infill pattern, tested at two different raster angles. The Samples printed with a 45° raster angle show lower strength and earlier breakage compared to the 90° counterpart. The 90° raster angle enhances the tensile strength across all infill densities, particularly noticeable at 90% infill. This suggests that aligning the print raster at 90° might be more effective in optimizing load distribution and enhancing interlayer adhesion, which are critical factors in increasing the tensile strength of the printed object.

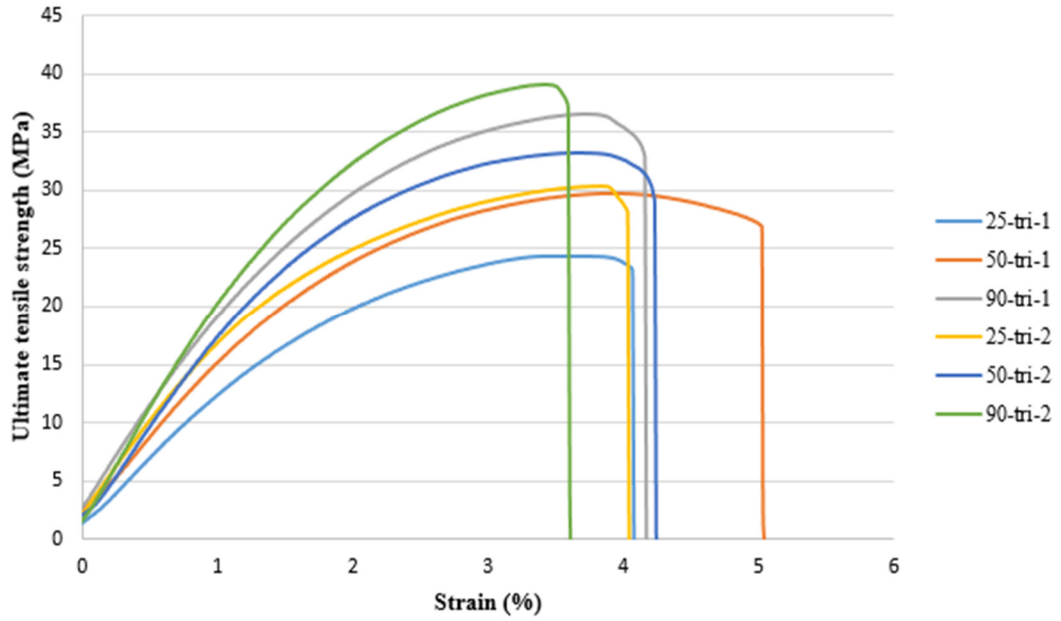

Figure 4.9: The results of ultimate tensile strength with different infill densities a) 25% b) 50% c) 90%, triangles as infill pattern with raster angle of 45 and 90°

Figure 4.9 shows the stress vs strain diagrams for the presented samples in Table 4.3. 90° a raster angle generally, the tensile strength at this angle is slightly higher than at 45°, Especially noticeable at higher densities (50% and 90%). This suggests that a 90° raster angle may align better with the loading direction in tensile testing, thus enhancing the effective strength of the material. The curves show a consistent growth in tensile strength as the infill density increases. The trend indicates that even at a 45° raster angle, increasing the infill density significantly boosts the material's mechanical properties.

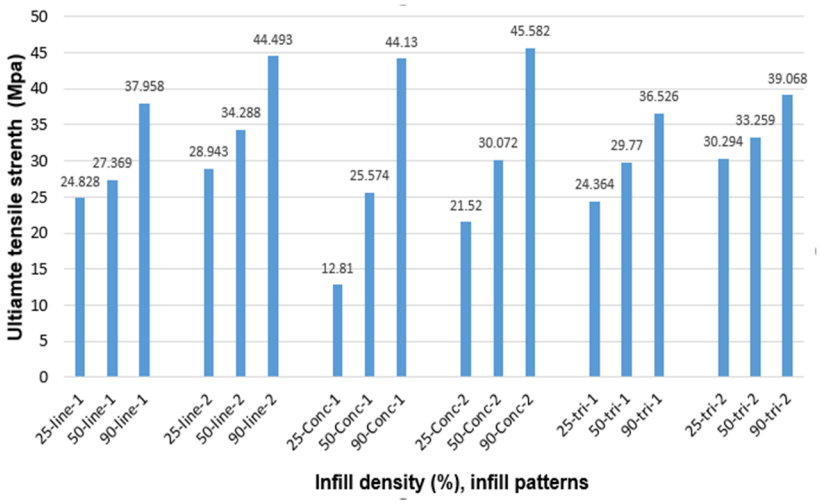

Figure 4.10: The results of all ultimate tensile strength versus infill density, infill pattern with raster angle of 45 and 90°

Understanding how different combinations of infill pattern, infill density, and raster angle affect the mechanical properties of 3D printed parts can be gained from analyzing Figure 4.10, which shows the ultimate tensile strength (UTS) outcomes. It can be seen that, for various infill patterns and densities, a 90º raster angle outperforms a 45° as raster angle.

Specimens with a concentric infill pattern at 90% infill density and a 90° raster angle had the highest Ultimate Tensile Strength (UTS) ever measured: 45.5 MPa. Among the variables tested, this combination performed the best in achieving maximal tensile strength. It demonstrates how optimizing raster angle orientation and infill density can improve material performance.

With a 45° raster angle and a concentric pattern with 25% infill density, the lowest UTS ever recorded was 12.8MPa. This demonstrates the material's minimal performance under the test conditions. When the UTS findings were sorted by infill pattern, the concentric pattern had the maximum strength of 45.5 MPa, followed by lines at 44.4 MPa.

Triangles had the lowest UTS among the best-performing shapes at 39.1 MPa. This ranking shows how the infill pattern shape efficiency influences the material and load distribution of the printed part.

The results of an inquiry into the ultimate tensile strength (UTS) of 3D printed materials clearly indicate the importance of adjusting process parameters. After testing and analyzing various designs, the following criteria were discovered to produce the most significant outcomes in terms of high tensile strength:

- Infill Density: 90% was the most efficient infill density. A high infill density increases the amount of material in the print, which lowers the part's chance of failing under tension and dramatically increases the part's strength.
- Infill Pattern: The best option was the concentric infill pattern. This design allows for better stress distribution across the part and improves the material's reaction to tensile stresses.
- Raster Angle: A raster angle of 90° was found to be optimal. This angle aligns the print layers more directly with the tensile forces applied during testing, helping achieve higher tensile strength.

4.5 The Results of Stiffness

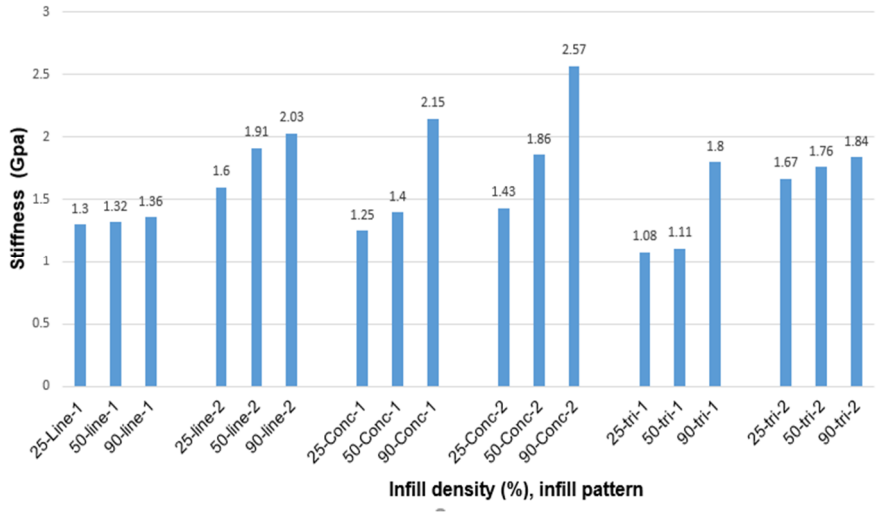

Figure 4.11: The results of all stiffness versus infill density, infill pattern with raster angle of 45 and 90°

The stiffness results of 3D-printed items are affected by various infill patterns and densities. Figure 4.11 provides a detailed analysis of how these variables interact to influence the structural rigidity of 3D-printed parts. According to the analysis, concentric patterns perform better than other patterns in terms of stiffness, achieving a 2.5 GPA, followed by lines at 2.0 GPA and triangles at 1.8 GPA. All patterns show a similar trend of increased stiffness with higher infill density, highlighting the essential function of material volume in improving part stiffness. The stiffness effectiveness ranking of infill patterns indicates that concentrated patterns are the most effective. This is because they can equally distribute stress, particularly in sections with complex shapes [30]. A distinct set of ideal settings has been identified as a result of tensile testing to establish the best 3D printing parameters for maximum material stiffness. These configurations, which result in the maximum stiffness, consist of:

- Infill Density: It was discovered that a high infill density of 90% worked best. By decreasing the amount of space where material can flex or deform under stress, this increased density usually results in more material within the printed structure, thereby increasing its stiffness and strength.
- Infill Pattern: The best infill pattern in terms of stiffness was found to be concentric. Because the design distributes stress uniformly throughout the print, stiffness benefits from it. The infill's circular shape probably helps to distribute loads more evenly, which is essential for minimizing weak spots and strengthening structural integrity.
- Raster Angle: The best raster angle was 90°. This orientation aligns the print layers directly with the direction of applied stress during testing, which helps to resist deformation more effectively. When the material deposition is parallel to the force applied, it often increases stiffness and strength properties.

4.6 Statistical Analysis of Ultimate Tensile and Stiffness Results

Table 4.4: The analysis of Variance (ANOVA) for the transformed response of UTS

Source	DF	Adj SS	Adj MS	F-Value	P-Value
Model	13	5069952	389996	39.39	0.001
Linear	5	4428683	885737	89.46	0.00
Infill density	2	4014551	2007276	202.73	0.00
Infill pattern	2	32602	16301	1.65	0.301
Raster angle	1	381529	381529	38.53	0.003
2-Way Interactions	8	641269	80159	8.10	0.030
Infill density * Infill pattern	4	616493	154123	15.57	0.010
Infill density * Raster angle	2	136	68	0.01	0.993
Infill pattern * Raster angle	2	24640	12320	1.24	0.380
Errors	4	39606	9901		
Total	17	5109558			
Model summary					
Standard deviation (S) = 99.5057					
R^2= 99.22%					
R^2_{Adj}= 96.71%					
R^2_{Pred}= 84.30%					

Table 4.4 shows the analysis of Variance of the presented ultimate tensile strength results.

Table 4.5: The analysis of Variance (ANOVA) for the transformed response of UTS after removing the non-significant effect

Source	DF	Adj SS	Adj MS	F-Value	P-Value
Model	9	5045176	560575	69.66	0.000
Linear	5	4428683	885737	110.06	0.000
Infill density	2	4014551	2007276	249.42	0.000
Infill pattern	2	32602	16301	2.03	0.194
Raster angle	1	381529	381529	47.41	0.000
2-Way Interactions	4	616493	154123	19.15	0.000
Infill density * Infill pattern	4	616493	154123	19.15	0.000
Errors	4	64381	8048		
Total	17	5109558			
Model summary					
Standard deviation (S) = 89.7088					
$\boldsymbol{R^2}$= 99.22%					
R^2_{Adj}= 97.32%					
R^2_{Pred}= 93.62%					

Table 4.5 shows the results of ANOVA; after removing non-significant effects based on the ANOVA for ultimate tensile strength (UTS), an improvement in the P-value column's significance was observed (Table 4.5), along with an increase in the predicted R-squared from 84.3% to 93.6%. This signifies a more refined and accurate model, highlighting several key points about the process and its implications.

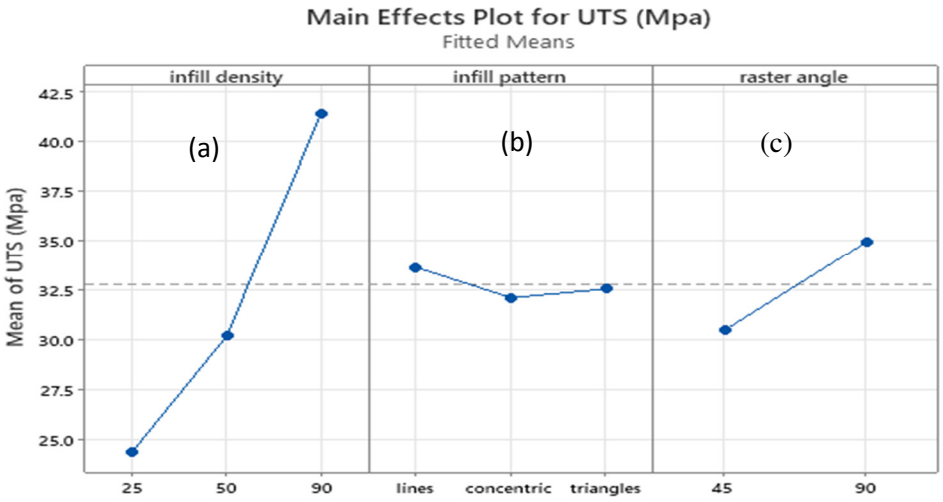

Figure 4.12: The main effects plot for ultimate tensile strength with process parameters of a) infill density, b) infill pattern, c) raster angle

Figure 4.12 depicts the main effects plot for Ultimate Tensile Strength (UTS), which examines the impact of infill density, infill pattern, and raster angle on 3D-printed components. The graphic clearly shows how each process parameter influences the UTS. Based on the description, we investigated the observed trends and their consequences.

a) Infill Density: The UTS increases with the infill density, reaching its peak at 90%. This is expected as higher infill densities mean more material is present within the part. This increased material offers excellent resistance to tensile forces and enhances the UTS. Thus, maximizing infill density to 90% is advisable, which gives better results.

b) Infill Pattern: Infill pattern does not significantly affect UTS. This suggests that within the range of patterns tested (lines, concentric, triangles), the UTS is relatively insensitive to the pattern type.

c) Raster Angle: The raster angle was 90°, resulting in an ultimate tensile strength greater than 45°. This result could be attributable to aligning the print lines with the direction of tensile forces, which improves layer adhesion and load distribution. As a result, a raster angle of 90º is preferred for maximizing UTS. This knowledge is especially useful for designing pieces that withstand significant tensile stress.

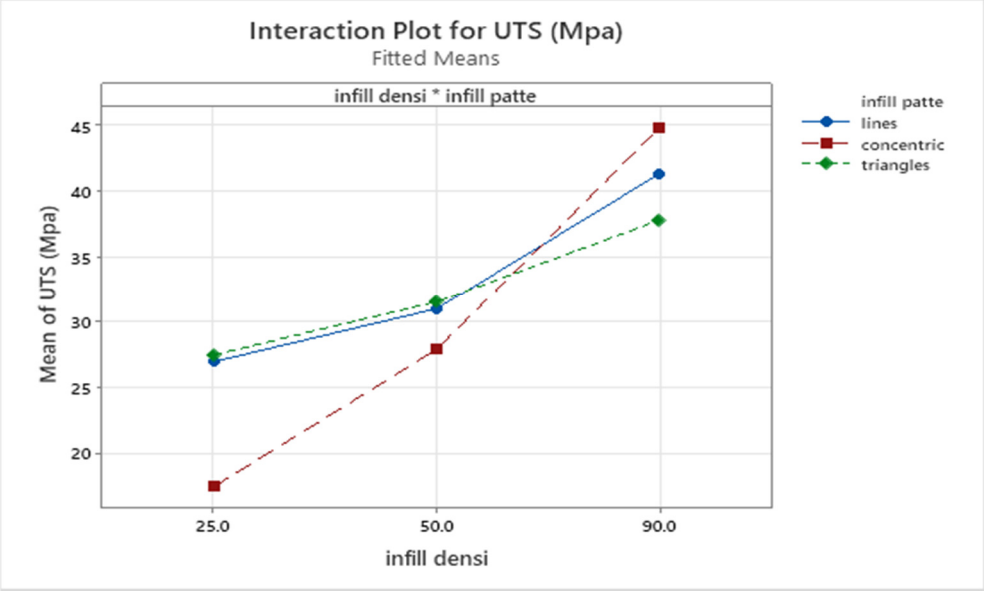

Figure 4.13: The interaction plot for the ultimate tensile strength of the infill pattern

The interaction plot shown in Figure 4.13 focuses on the impact of infill patterns and other process parameters on ultimate tensile strength (UTS). The plot shows that the concentric pattern yields the highest UTS, making it more effective than other patterns. The concentric pattern is particularly useful in distributing tensile forces throughout the part. The uniform support and stress distribution provided by this arrangement can be especially beneficial under uniform or radially symmetric loading conditions.

Table 4.6: The analysis of Variance (ANOVA) for the transformed response of stiffness

Source	DF	Adj SS	Adj MS	F-Value	P-Value
Model	9	2.7178	0.30198	15.17	0.000
Linear	5	2.2347	0.44693	22.45	0.000
Infill density	2	1.1566	0.57832	29.05	0.000
Infill pattern	2	0.1212	0.06062	3.05	0.104
Raster angle	1	0.9568	0.95681	48.07	0.000
2-Way Interactions	4	0.4831	0.12078	6.07	0.015
Infill density * Infill pattern	4	0.4831	0.12078	6.07	0.015
Errors	4	0.1592	0.01991		
Total	17	2.8771			
Model summary					
Standard deviation (S) = 0.141087					
$\boldsymbol{R^2}$= 94.47%					
R^2_{Adj}= 88.24%					
R^2_{Pred}= 71.98%					

Table 4.6 depicts the basic purpose of determining the parameters that significantly affect the stiffness of a material or component by studying the P-values associated with each factor. The improved ANOVA model becomes more accurate and focused and provides better statistical evidence for the relevant stiffness-influencing components.

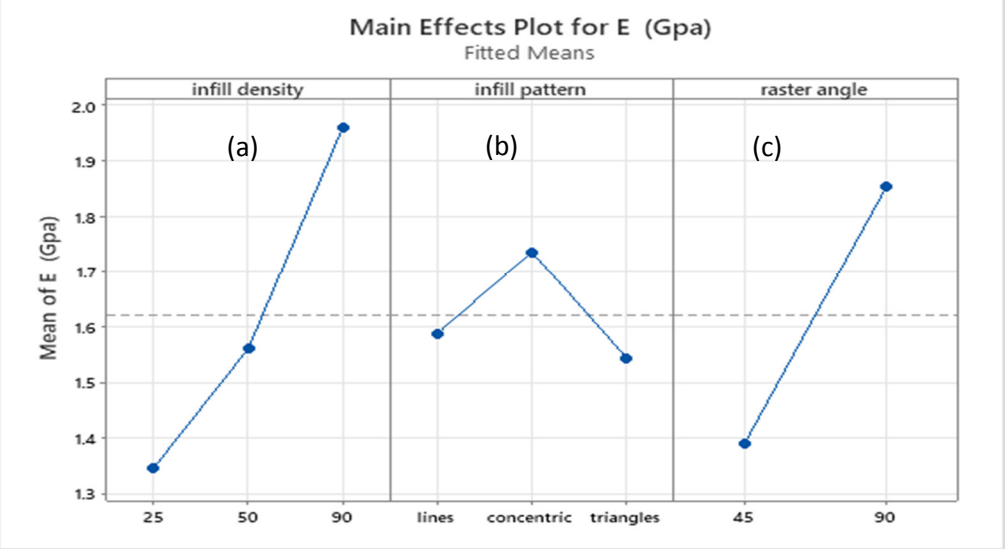

Figure 4.14: The main effects plot for stiffness with process parameters of a) infill density, b) infill pattern, c) raster angle

The main effect plot for stiffness, analyzed through process parameters such as infill density, infill pattern, and raster angle, provides valuable insights into optimizing 3D printing settings to maximize stiffness.

Figure 4.14 a) represents that infill density, set at 25%, 50%, and 90%, significantly affects the internal structure of printed parts. Higher densities increase the material volume within the part, potentially enhancing its stiffness by providing more resistance against bending and deformation. According to these infill density tests, 90% was chosen to give better results.

Figure 4.14 b) shows that the choice of infill pattern - lines, concentric, and triangles can influence how the material is distributed throughout the part, affecting its ability to distribute stress and, consequently, its stiffness. The concentric pattern shows high stiffness compared to others.

Figure 4.14 c) represents that the orientation of the print layers relative to the part's geometry can affect layer adhesion and the part's overall structural integrity. According to the results presented, printing at a 90º raster angle leads to higher stiffness.

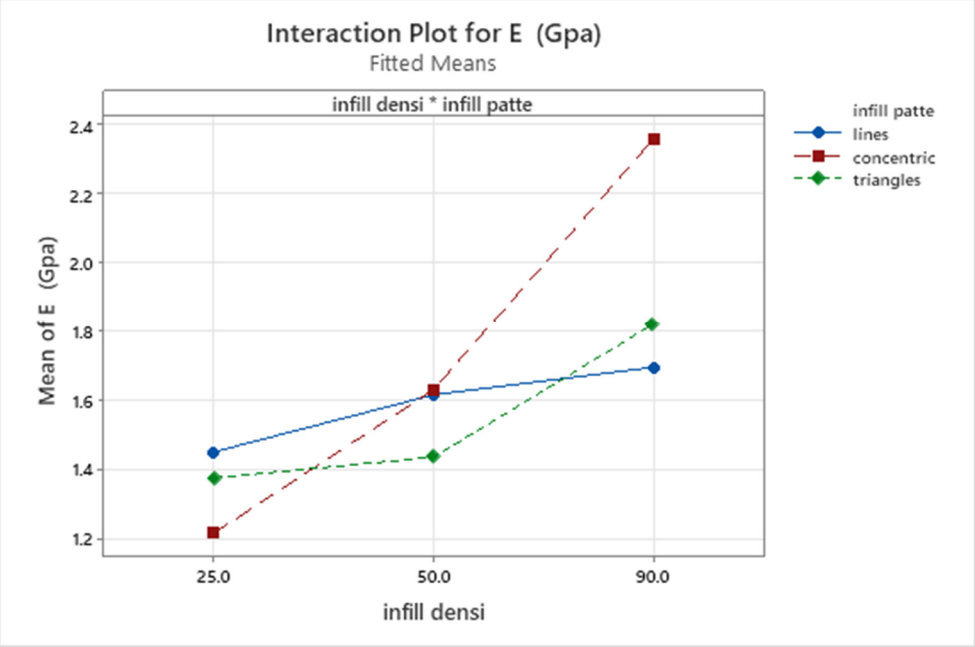

Figure 4.15: The interaction plot for stiffness of the infill pattern

Figure 4.15 shows the interaction of the parameters on the stiffness of the printed parts. The concentric infill pattern, which is effective for material distribution and structural support, results in the highest stiffness and performance. The reason for this is its capacity to distribute stress effectively. The interaction plot indicates that the concentric infill pattern improves the stiffness of 3D-printed objects by providing uniform support and effectively distributing tensile forces.

4.7 Bending Test

Figure 4.16 shows the three-point bending tests performed on the produced samples in accordance with ASTM D790 using the universal tensile test machine. The ASTM D790 standard specifies how to determine the flexural properties of both unreinforced and reinforced polymers, as well as electrical insulating materials.

Figure 4.16: The three-point bending test of PA12-CF as a sample according to the ASTM D790

This experiment investigates how three process parameters, including infill density, infill pattern, and raster angle, influence the flexibility of 3D-printed objects. We printed 18 specimens. The testing beams have the following dimensions: 140mm support span, 13mm width, and 4mm thickness (Figure 4.17).

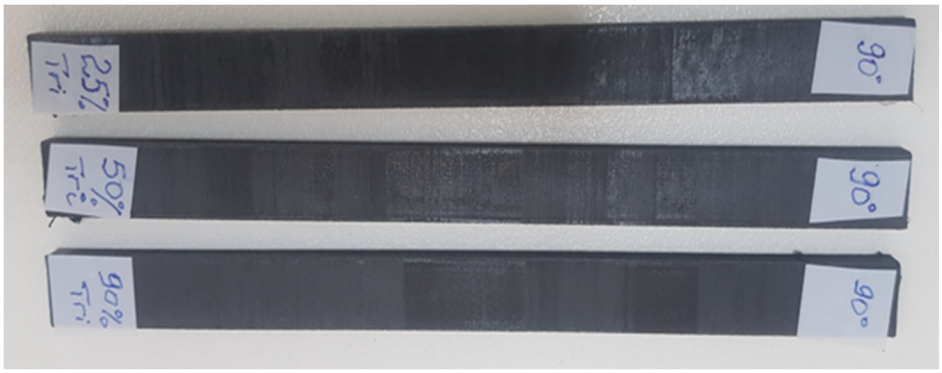

Figure 4.17: Representation of the printed part

4.8 The Results of Flexural Stress and Stiffness

The test method in this study enables accurate determination of the maximum flexural stress, or the highest stress the material experiences at the outermost fiber on the tension side immediately before failure.

Equations 1,2 and 3 were used to calculate the flexural stress and strain, and stiffness , respectively [49].

Flexural stress:

$$\sigma_f = \frac{3PL}{2bd^2} \quad (1)$$

Where:

σ = stress in the outer fibers at the midpoint, (Mpa)

P = load at a given point on the load-deflection curve, (N)

L = support span,(mm)

b = width of beam tested, (mm) , and

d = depth of beam tested, (mm)

Flexural strain:

$$\varepsilon_f = \frac{6Dd}{L^2} \quad (2)$$

Where:

ε_f = strain in the outer surface, (mm/mm)

D = maximum deflection of the center of the beam, (mm)

L = support span, (mm), and

d = depth, mm of beam tested, (mm)

Flexural stiffness:

$$E_B = \frac{L^3 m}{4bd^3} \quad (3)$$

Where:

E_B= Modulus of elasticity in bending, (Mpa)

L= Support span, (mm)

b= Width of beam tested, (mm)

d= Depth of beam tested, (mm)

m= Slope of the tangent to the initial straight-line portion of the load-deflection curve, (N/mm)

Table 4.7 shows all results of flexural stress in all 18 specimens as shown below:

Table 4.7: The results of flexural stress and stiffness

No	Sample ID	Infill density (%)	Infill pattern	Raster angle (Degree)	Flexural stress (MPa)	Flexural stiffness (Gpa)
1	25-Line-1	25	Lines	45º	49.4	2.9
2	50-Line-1	50	Lines	45º	52.5	2.8
3	90-Line-1	90	Lines	45º	53.5	2.2
4	25-Line-2	25	Lines	90º	57.5	3.5
5	50-Line-2	50	Lines	90º	67.6	3.9
6	90-Line-2	90	Lines	90º	81.7	4.2
7	25-Concentric-1	25	Concentric	45º	52.4	3.2
8	50-Concentric-1	50	Concentric	45º	57.3	3.25
9	90-Concentric-1	90	Concentric	45º	59.6	3.8
10	25-Concentric-2	25	Concentric	90º	51.5	3.3
11	50-Concentric-2	50	Concentric	90º	53.5	3.2
12	90-Concentric-2	90	Concentric	90º	66.6	2.0
13	25-Triangle-1	25	Triangles	45º	51.4	3.0
14	50-Triangle-1	50	Triangles	45º	59.5	3.5
15	90-Triangle-1	90	Triangles	45º	68.6	3.9
16	25-Triangle-2	25	Triangles	90º	58.5	3.9
17	50-Triangle-2	50	Triangles	90º	70.7	4.5
18	90-Triangle-2	90	Triangles	90º	75.7	5.1

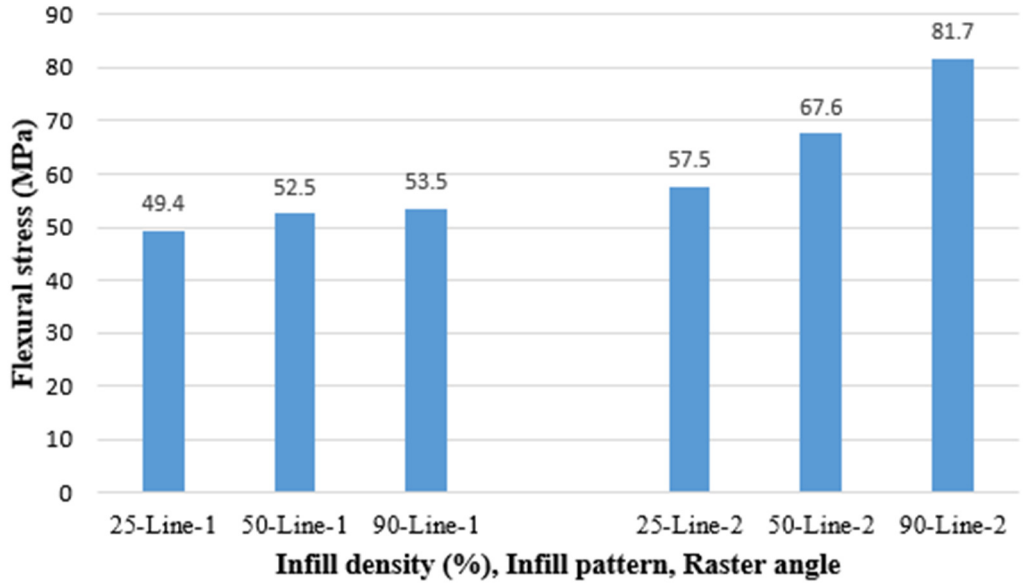

Figure 4.18: Results of flexural stress as infill pattern lined with different infill densities: a) 25%, b) 50%, c) 90%, and raster angles of 45° and 90°

Figure 4.18 shows the results of a bending test (flexural stress) for specimens with different infill densities (25%, 50%, 90%) and two raster angles (45 and 90°), all using a line infill pattern and increasing the raster angle from 45 to 90° increased flexural stress, suggesting better resistance to bending but at a cost of reduced flexural strain, indicating a stiffer but slightly more brittle behavior. A higher raster angle increased flexural stress, significantly improving structural integrity under bending. However, the lower strain at higher raster angles suggests increased material strain and potential brittleness. For 90% infill, a raster angle of 90° not only substantially increased flexural stress but maintained a higher strain than the other high-density configurations, indicating a well-balanced approach between strength and ductility.

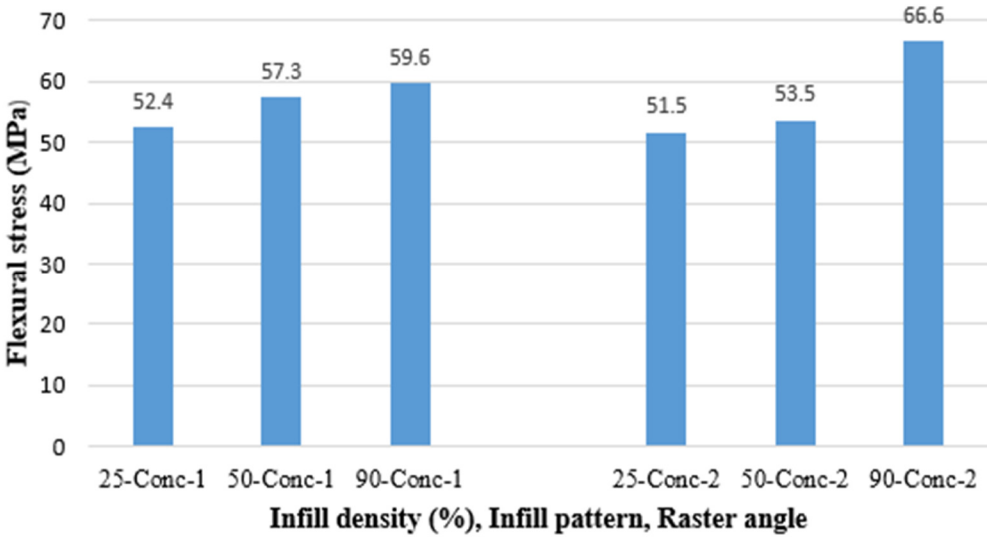

Figure 4.19: Results of flexural stress as infill pattern were concentric with different infill densities: a) 25%, b) 50%, c) 90%, and raster angles of 45° and 90°

Figure 4.19 illustrates the results of a bending test (flexural stress) focusing on 3D printed parts using a concentric infill pattern with varying infill densities (25%, 50%, 90%) and two different raster angles (45 and 90°) and providing insight into the mechanical behavior of the materials under bending loads. An increase in raster angle from 45 to 90° leads to higher flexural stress, indicating improved structural integrity but a decrease in flexural strain, suggesting reduced material ductility.

An increase in the raster angle improves the flexural stress and the flexural stiffness, which is atypical. This suggests that the concentric pattern at a 90° angle may enhance load distribution capabilities, leading to higher strength and increased flexibility. The 90° raster angle significantly enhances stress and strain outcomes, indicating optimal performance in strength and elasticity at high infill densities with a 90° raster setting.

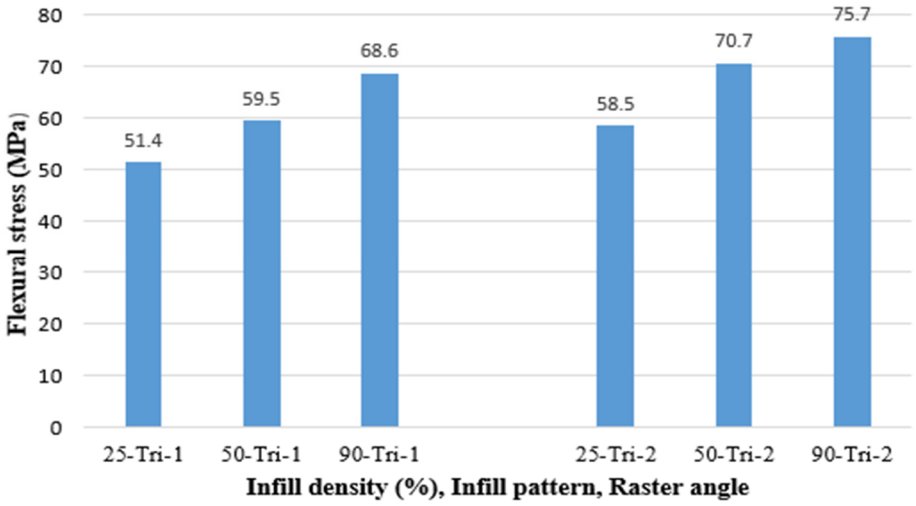

Figure 4.20: Results of flexural stress as infill pattern were triangles with different infill densities: a) 25%, b) 50%, c) 90%, and raster angles of 45° and 90°

Figure 4.20 presents results from a flexural test analyzing 3D-printed parts with triangular infill patterns across varying infill densities and raster angles. Increasing the raster angle from 45 to 90° results in higher flexural stress, suggesting improved material rigidity. Increasing the raster angle for 50% infill density enhances the flexural stress, indicating stronger material behavior under bending. At the highest infill density of 90%, the increase in raster angle continues to significantly improve flexural stress, marking the strongest material resistance among the tested groups.

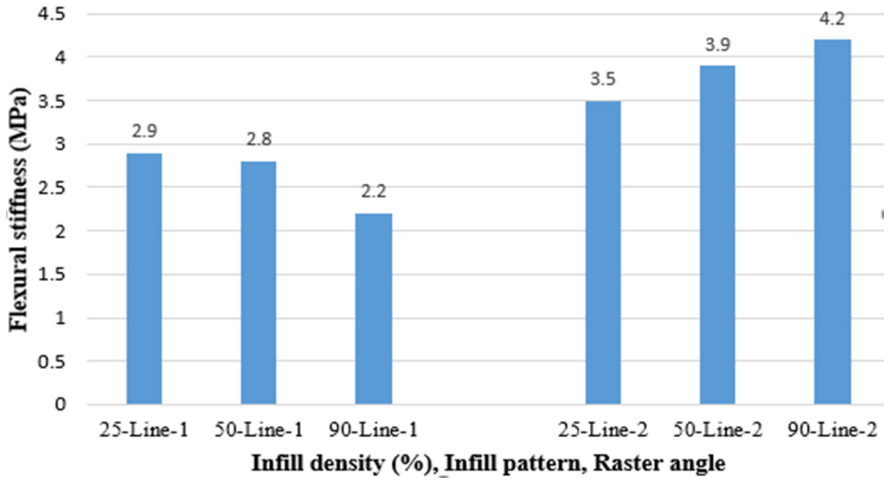

Figure 4.21: Results of flexural stiffness as infill pattern were lines with different infill densities: a) 25%, b) 50%, c) 90%, and raster angles of 45° and 90°

Figure 4.21 illustrates the flexural stiffness (in MPa) of 3D-printed PA12-CF samples with line infill patterns. The results indicate that increasing the raster angle from 45º to 90° consistently improves the flexural stiffness across all infill densities. At a 90° raster angle, the infill density of 90% demonstrates the highest flexural stiffness of 4.2GPa, suggesting a strong correlation between higher infill density and improved mechanical properties. Conversely, the infill density of 90% at a 45° raster angle results in the lowest flexural stiffness of 2.2GPa, indicating the significant impact of the raster angle on mechanical performance.

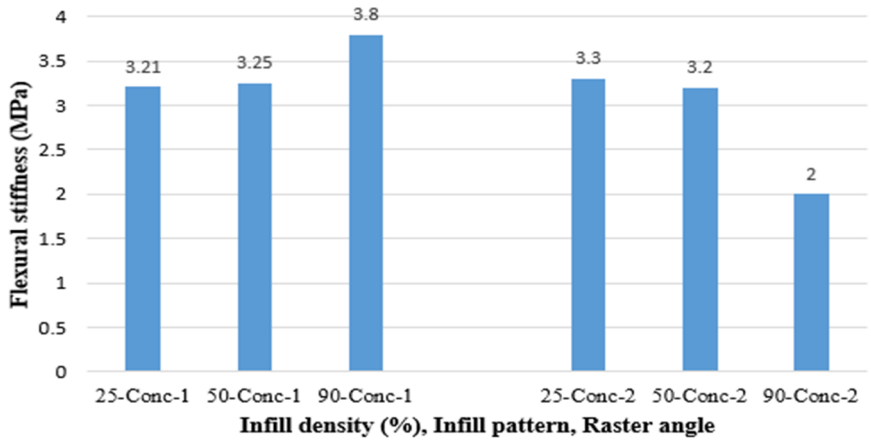

Figure 4.22: Results of flexural stiffness as infill pattern were concentric with different infill densities: a) 25%, b) 50%, c) 90%, and raster angles of 45° and 90°

Figure 4.22 shows that flexural stiffness generally increases with higher infill densities when using a raster angle of 45°, with the maximum stiffness observed at a 90% infill density. For the 90° raster angle, the highest flexural stiffness is observed at a 25% infill density, whereas the lowest stiffness is recorded at a 90% infill density. The concentric infill pattern with a raster angle of 45° consistently provides higher flexural stiffness than the 90° raster angle across all infill densities. The optimal flexural stiffness is achieved with an infill density of 90%, a concentric infill pattern, and a raster angle of 45°, yielding a flexural stiffness of 3.8GPa. This result emphasizes the significant influence of infill density and raster angle on the mechanical properties of 3D-printed parts. The concentric pattern effectively aligns with the direction of applied loads, enhancing the material's ability to resist bending and deformation.

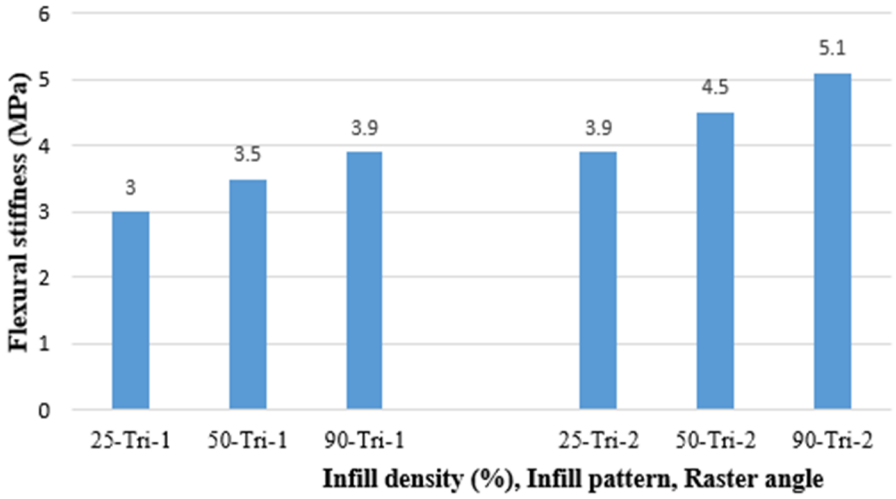

Figure 4.23: Results of flexural stiffness as infill pattern were triangles with different infill densities: a) 25%, b) 50%, c) 90%, and raster angles of 45° and 90°

Figure 4.23 shows flexural stiffness generally increases with higher infill densities for 45° and 90° raster angles. The highest flexural stiffness was observed at a 90% infill density and 90° raster angle of 5.1GPa, indicating the significant influence of both high infill density and optimal raster angle on mechanical performance.

The triangular infill pattern with a 90° raster angle consistently provides higher flexural stiffness than the 45° raster angle across all infill densities.

The optimal flexural stiffness is achieved with an infill density of 90%, a triangular infill pattern, and a raster angle of 90°, yielding a flexural stiffness of 5.1GPa. This result underscores the importance of both high infill density and appropriate raster angle in maximizing the mechanical properties of 3D-printed parts. The triangular infill pattern, known for its geometric efficiency, contributes to superior mechanical properties by providing a strong and stable internal lattice structure. The alignment of the pattern with the 90° raster angle optimizes load transfer and minimizes stress concentrations, resulting in higher flexural stiffness.

Table 4.8: The analysis of variance (ANOVA) for the transformed response of flexural stress

Source	DF	Adj SS	Adj MS	F-Value	P-Value	Remarks
Model	5	20330009	4066002	4.12	0.021	Significant
Linear	5	20330009	4066002	4.12	0.021	Significant
Infill density	2	6052788	3026394	3.07	0.084	Not significant
Infill pattern	2	3070550	1535275	1.56	0.251	Not significant
Raster angle	1	11206672	11206672	11.35	0.006	Significant
Errors	4	11843877	986990			
Total	17	32173886				
S= 0.099						
R^2= 65.19%						

The ANOVA findings are also displayed in Table 4.8; these results suggest that although the overall model significantly predicts flexural stress, individual components such as pattern and infill density are not statistically significant at usual thresholds. However, the raster angle demonstrates a substantial influence, emphasizing its importance in controlling the material's flexural properties. This analysis underscores the critical role of raster orientation in the structural behavior of materials under flexural stress, which can be essential for optimizing manufacturing processes or enhancing material performance in practical applications.

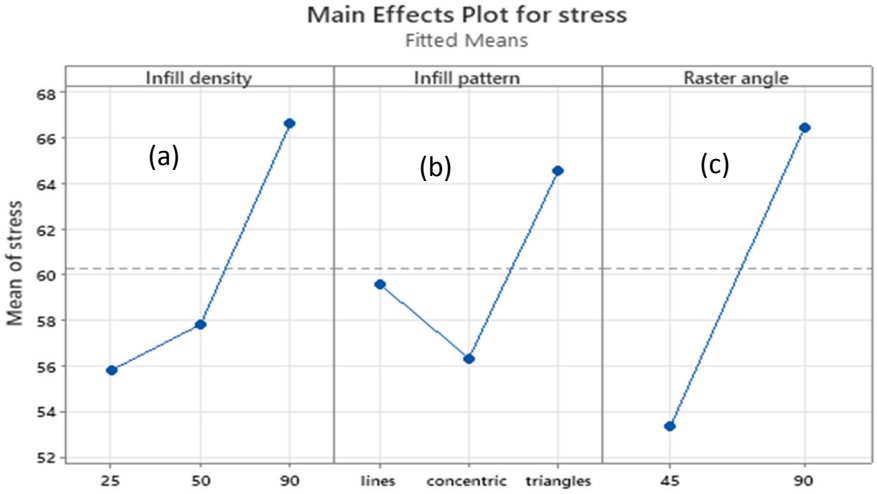

Figure 4.24: presentation of main effects plots for flexural stress with different process parameters: a) infill density, b) infill pattern, c) raster angle

Figure 4.24 provides a “Main Effects Plot for flexural stress,” which graphically represents the effects of three different process parameters on the mean of flexural stress in a scientific study likely focused on materials used in additive manufacturing.

Figure 4.24 (a) shows a clear upward trend in flexural stress as infill density increases from 25% to 90%. At 25%, the mean stress is the lowest, increasing substantially at 50% and peaking at 90%. This indicates that higher infill densities significantly enhance the material's stiffness and ability to bear higher flexural loads. The increase in density likely results in less porosity within the material, providing more continuous material characteristics that resist deformation under stress.

Figure 4.24 (b) demonstrates a varied response. The lines pattern shows the lowest stress, whereas the concentric pattern exhibits a significant stress reduction compared to the lines. However, the triangle pattern results in the highest flexural stress. This variation suggests that the geometric arrangement of the infill can significantly influence how the material distributes and withstands stress. Triangular patterns, known for their high geometric stability and effective load distribution, clearly provide superior performance in enhancing the material’s response to flexural forces.

Figure 4.24 (c) presents the significant influence of raster angle on flexural stress. At 45°, the stress levels are comparatively lower, increasing markedly when the raster angle is adjusted to 90°. This effect can be attributed to the alignment of the material deposition relative to the direction of the applied load. A 90° likely aligns more effectively with the force application, optimizing load bearing and reducing the likelihood of material failure under stress.

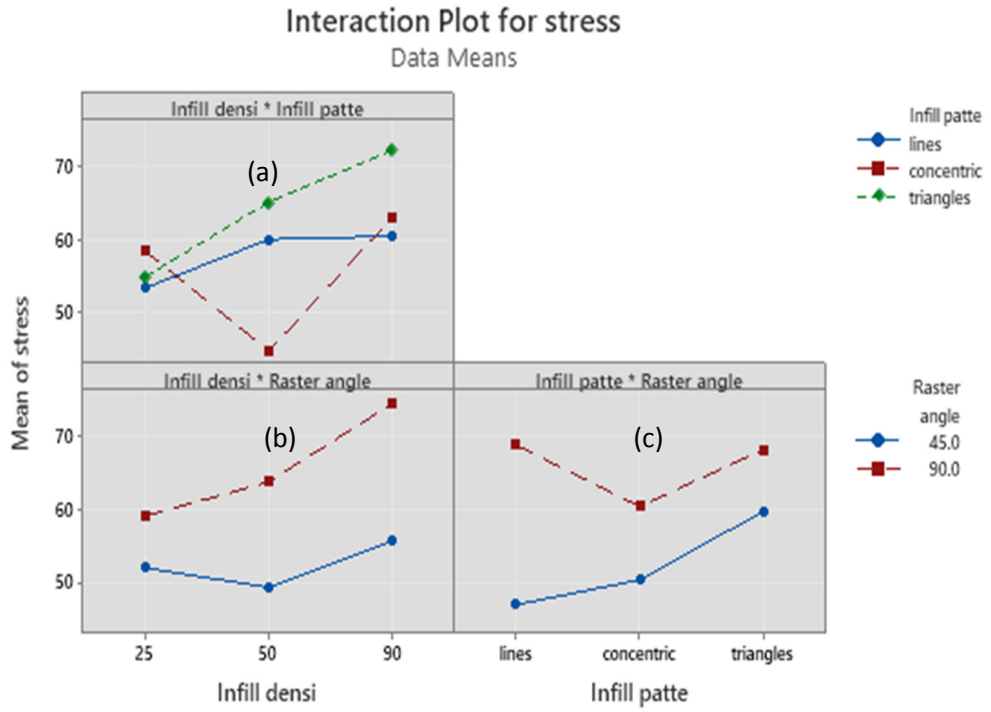

Figure 4.25: presentation of interaction plot for flexural stress with different process parameters: a) infill density, b) infill pattern, c) raster angle

Figure 4.25 elucidates how these parameters interactively influence material performance under bending loads.

Figure 4.25 (a) shows that increasing infill density, infill pattern generally results in higher stress values across all infill patterns. This aligns with expectations that more material contributes to greater structural integrity. The triangle pattern consistently demonstrates the highest stress increase with infill density, followed by concentric lines. This suggests that the triangular pattern most effectively leverages increased material density to enhance stress resistance, likely due to its geometric stability and efficient load distribution.

Figure 4.25 (b) shows infill density and raster angle. Increasing infill density enhances flexural stress, but the increase is more pronounced at a 90° raster angle. This indicates that the orientation of material deposition at 90° is more effective in resisting bending stresses, particularly at higher densities.

Figure 4.25 (c) infill pattern, raster angle shows variable responses with different raster angles, where the stress values do not exhibit a consistent trend, suggesting that these patterns might not be as effective in utilizing the raster angle for stress resistance. The triangle pattern significantly increases stress values as the raster angle changes from 45° to 90°. This highlights that the triangular pattern and a perpendicular raster angle optimally align the material deposition to bear and distribute the load effectively.

Table 4.9: The analysis of variance (ANOVA) for the transformed response of flexural strain

Source	DF	Adj SS	Adj MS	F-Value	P-Value	Remarks
Model	5	0.061415	0.012283	8.19	0.001	Significant
Linear	5	0.061415	0.012283	8.19	0.001	Significant
Infill density	2	0.006749	0.003375	2.25	0.148	Not significant
Infill pattern	2	0.034659	0.017329	11.55	0.002	Significant
Raster angle	1	0.020007	0.020007	13.34	0.003	Significant
Errors	4	0.017998	0.001500			
Total	17	0.079413				
S= 0.078						
R^2= 77.34%						

Table 4.9 examines the effects of various parameters, including infill density, infill pattern, and raster angle. Although infill density contributes to the model, it is not statistically significant (p-value = 0.148). This shows that variations in infill density have no significant effect on flexural strain within the measured range. On the other hand, the infill pattern is significant (p-value = 0.002), showing a major influence on the flexural strain. This is most likely owing to variations in material distribution and structural properties associated with different patterns.

Similarly, the raster angle has a significant effect (p-value = 0.003), indicating that the angle of material deposition determines how the material reacts to flexural stress. In general, the ANOVA results show that, while infill density has no significant effect on flexural strain on its own, both infill pattern and raster angle play important roles in defining the behavior of materials under flexural stress.

This means optimizing these factors may improve the performance characteristics of materials used in additive manufacturing, particularly their capacity to withstand flexural loads.

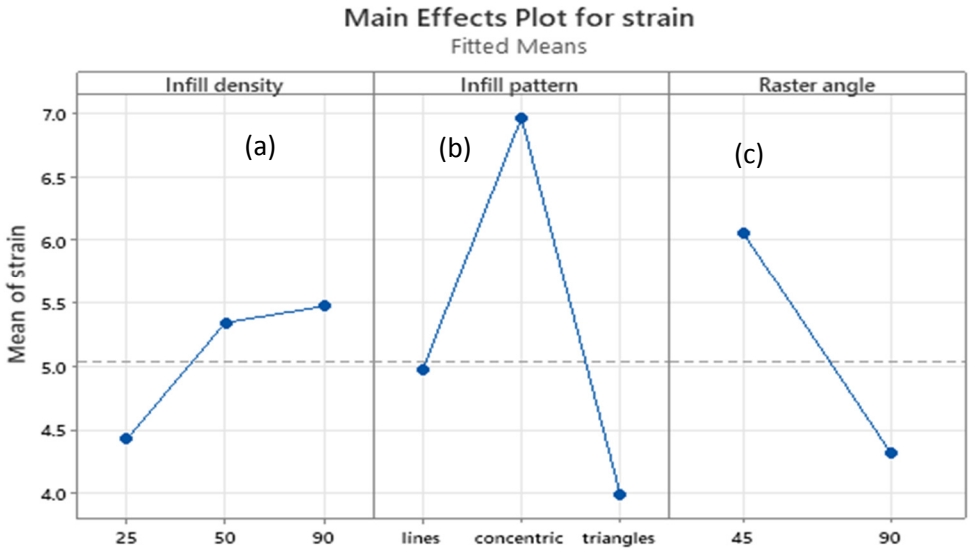

Figure 4.26: presentation of main effects plots for flexural strain with different process parameters: a) infill density, b) infill pattern, c) raster angle

Figure 4.26 illustrates the impact of three process parameters - infill density, infill pattern, and raster angle - on the mean flexural strain observed in a material. Each of these parameters is analyzed for their influence on the material's deformation under flexural loading. To select the best suitable parameter, we consider the one that produces maximum flexural strain as follows:

Figure 4.26 (a) shows the highest flexural strain observed at a 90% infill density. Higher densities usually make stiffer materials less capable of distributing stress flexibly under load, leading to higher strain when they deform. This can be useful in scenarios where strain measurements are critical for performance assessments or where a certain level of material deformation is required for functionality.

Figure 4.26 (b) demonstrates that the concentric pattern shows the highest peak in strain among the infill patterns analyzed. The concentric pattern, involving circular or spiral configurations, may induce uneven stress distributions under certain loading

conditions, leading to higher overall strain. This pattern can be advantageous in applications where materials must undergo significant but controlled deformation before failure.

Figure 4.26 (c) shows that a raster angle 45° is associated with higher strain than 90°. At 45°, the material layout may interact more complexly with applied forces, leading to greater deformation. This angle might benefit applications requiring greater material flexibility or where a material's deformation characteristics are critical to its performance.

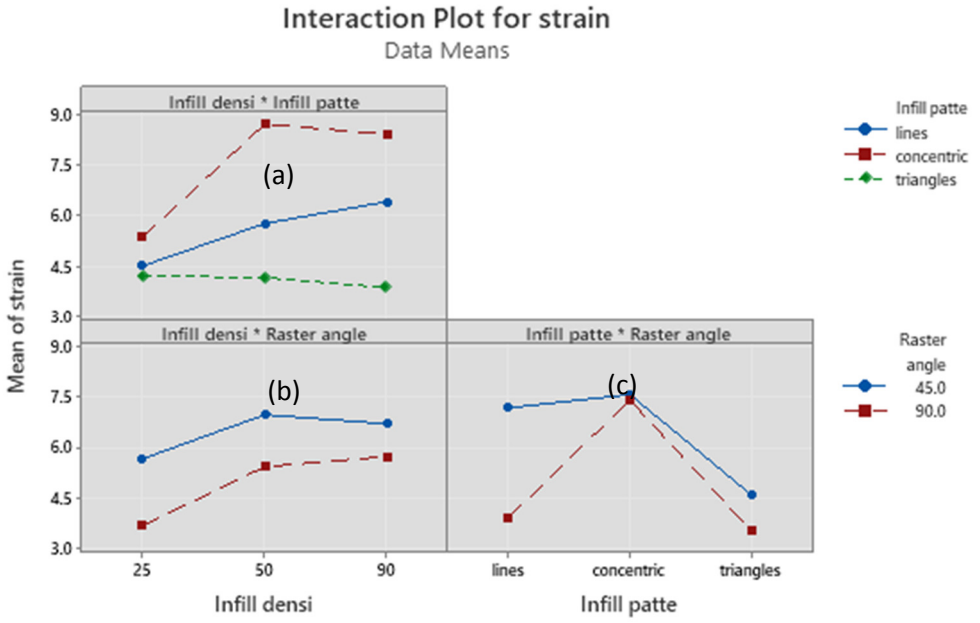

Figure 4.27: presentation of interaction plot for flexural strain with different process parameters: a) infill density, b) infill pattern, c) raster angle

Figure 4.27 shows the effects of infill density, infill pattern, and raster angle on flexural strain, illustrating how these parameters interactively influence the material's deformation characteristics under stress.

Figure 4.27 (a), the infill density, infill pattern presents the best infill density of 90%. This density increases the material bulk within the print, reducing the presence of voids and enhancing the object's overall mass and structural integrity. At 90%, the

material is densely packed, which typically contributes to increased stiffness. However, in the context of flexural strain, this density allows for a significant but controlled deformation under load before reaching failure, as the material has enough continuity and connectivity to support deformative stress.

Figure 4.27 (b), infill density, raster angle indicates that the best angle was 45°. A 45° angle results in material layers that are obliquely aligned concerning the load. This orientation can increase the material's exposure to shear forces, potentially contributing to greater overall strain as the material tries to accommodate both bending and shearing actions.

Figure 4.27 (c) shows the infill pattern and raster angle, showing that the best infill pattern was concentric. Concentric patterns consist of continuous loops or rings that emanate outward from a central point. This configuration is advantageous for distributing stress evenly across the material. When flexural loads are applied, the concentric arrangement helps distribute these forces in a balanced manner along the contours of the pattern, potentially allowing for greater uniform deformation without localized stress concentrations that might lead to premature failure.

4.9 Response Optimization of Flexural Stress and Stiffness

Table 4.10 illustrates the goals for response optimization concerning two mechanical properties: flexural stiffness and stress. In materials science and engineering, optimizing these responses involves adjusting material properties and process parameters to meet specific performance targets under flexural loading conditions.

Table 4.10: Representation of response optimization of flexural stress and stiffness

Response	Goal	Lower	Upper	Weight	Importance
Stiffness	Maximize	2.0	5.1	1	1
Stress	Maximize	49.4	81.7	1	1

Table 4.11: Optimized parameter set obtained from analysis

Solution	Infill density (%)	Infill pattern	Raster angle (°)	Flexural Stiffness (Gpa)	Flexural Stress (MPa)	Composite desirability
1	90	Concentric	45°	5.1	81.7	0.66

Better visual identification of the impact of process factors as distinct plots is provided by response methodology, and dataset analysis results in a lucid conclusion. Additionally, we employ a tool response optimizer to determine the optimal process parameters that can yield the best flexural stress and strain output with optimistic inputs using the MINITAB 21.1.0 software. The improved input process parameter values from the statistical analysis are displayed in Table 4.11. The maximum values we were able to acquire in experimental work were 5.1Gpa of anticipated flexural stiffness where the infill density was 90%, the infill pattern was a triangle, and raster angle of 90° and 81.7 Mpa of flexural stress when the infill density was 90%, the infill pattern was lined, and the raster angle was 90°.

CHAPTER 5

CONCLUSION

5.1 Key Findings and Outcomes

The research demonstrated that specific adjustments in FDM process parameters substantially improve the performance of 3D-printed composites. Each conclusion serves a particular aspect of 3D printing optimization.

- Warpage Minimization: By setting the infill density at 90%, using a lined infill pattern, employing a flat printing direction, and fixing the raster angle at 90°, the warpage was effectively minimized to as low as 0.9mm. This configuration ensures maximum material continuity and stability during cooling, significantly reducing the internal stresses that cause warpage.
- Deviation Angle Reduction: Adjusting the infill density to 25%, adopting a triangular infill pattern, printing on edge, and maintaining a raster angle of 90°, the deviation angle was reduced to an impressive 0.04°. This setup likely favors precision in geometrical conformity, which is crucial for components requiring high alignment accuracy, such as camera holders.
- Maximization of Tensile Strength: A configuration of 90% infill density with a concentric pattern and a raster angle of 90° significantly increased the ultimate tensile strength to 45.5MPa. This indicates that a high density combined with a pattern that provides balanced stress distribution significantly enhances the load-bearing capacity of the printed parts.
- Stiffness Enhancement: Similarly, the same settings that maximized tensile strength also led to the highest measured stiffness of 2.5GPA. The concentric pattern at high infill densities optimizes the material's response to elastic deformation, providing substantial resistance to bending and other forms of mechanical stress.

These results underscore the importance of a holistic approach to parameter selection in FDM processes. The study contributes to the practical field of 3D printing by enhancing part quality and performance.

It provides a detailed guideline for manufacturers to tailor their printing strategies to specific mechanical requirements. This leads to more reliable and efficient production outcomes in industries where precision and mechanical robustness are paramount.

The study concludes how various process parameters influence warpage in thin-walled FDM-printed parts using carbon fiber-reinforced filament. By conducting simulations with DIGIMAT-AM software, which took into account process temperatures, material thermal properties, and slicing G-codes, valuable insights were gleaned about the optimal settings for minimizing warpage:

- Effectiveness of Line Patterns: The findings highlighted that balanced line patterns significantly minimize warpage. This is likely due to the even distribution of material and consistent thermal behavior during the printing process, which helps maintain the part's structural integrity.
- Challenges with Concentric Patterns: In contrast, concentric patterns, which are unbalanced, were shown to induce more significant warpage, particularly at higher infill densities. This effect is probably due to the uneven distribution of material and localized variations in cooling and contraction, which generate stresses that deform the part.

5.2 Future Works

The study's findings delve into the impact of printing orientation and parameter interactions on warpage in Fused Deposition Modeling Fabrication (FDM) of carbon fiber-reinforced polyamide 612. Future research aims to further these insights into more sophisticated, quantitatively driven realms to enhance Fused Deposition

Modeling technologies' precision, efficiency, and utility in high-stakes industries like aerospace and aviation. Here are the key areas for future research:

- Development of Predictive Models: Future research must focus on developing predictive models that can simulate and predict the outcomes of various fuse deposition Modeling settings in real-time. These models would integrate advanced analytics, machine learning algorithms, and real-time monitoring data to predict warpage and other potential print defects based on current print conditions and settings.
- Quantitative Analysis of Parameter Interactions: Further studies should aim to quantitatively analyze the complex interactions between Fused Deposition Modeling parameters such as infill density, pattern, printing speed, temperature settings, and material flow rates. This analysis would provide a more detailed understanding of how these variables work together in diverse printing scenarios.
- Real-Time Parameter Adjustment: Research into real-time parameter adjustment systems could revolutionize Fused Deposition Modeling by automatically allowing printers to adjust settings in response to predictive model feedback.
- Material Science Innovations: Further exploration into the material science aspects of filament composition, particularly for high-performance composites, could yield new filaments designed to minimize warpage and enhance print quality.
- Application-Specific Studies: Tailored studies focusing on specific applications within aerospace and aviation could help refine the use of Fused Deposition Modeling in these sectors. By addressing these areas, future research can provide significant advancements in the understanding and capabilities of Fused Deposition Modeling, paving the way for its expanded use in critical manufacturing processes where precision and reliability are paramount.

REFERENCES

[1] Pejkowski, Ł., et al., Mechanical performance of non-reinforced, carbon fiber reinforced and glass bubbles reinforced 3D printed PA12 polyamide. Polymer Testing, 2023. 118: p. 107891.

[2] Syrlybayev, D., et al., Optimisation of Strength Properties of FDM Printed Parts-A Critical Review, Polymers (2021), 13, 1587. 2021, s Note: MDPI stays neutral with regard to jurisdictional claims in published.

[3] De Laurentis, K.J. and C. Mavroidis, Rapid fabrication of a non□assembly robotic hand with embedded components. Assembly Automation, 2004. 24(4): p. 394-405.

[4] Sood, A.K., R. Ohdar, and S.S. Mahapatra, Improving dimensional accuracy of fused deposition modelling processed part using grey Taguchi method. Materials & design, 2009. 30(10): p. 4243-4252.

[5] Hopkinson, N., R. Hague, and P. Dickens, Rapid manufacturing: an industrial revolution for the digital age. 2006: John Wiley & Sons.

[6] Moylan, S., et al., An additive manufacturing test artifact. Journal of research of the National Institute of Standards and Technology, 2014. 119: p. 429.

[7] Armillotta, A., M. Bellotti, and M. Cavallaro, Warpage of FDM parts: Experimental tests and analytic model. Robotics and Computer-Integrated Manufacturing, 2018. 50: p. 140-152.

[8] Fitzharris, E.R., et al., Effects of material properties on warpage in fused deposition modeling parts. The International Journal of Advanced Manufacturing Technology, 2018. 95: p. 2059-2070.

[9] Yasa, E. and K. Ersoy, Dimensional accuracy and mechanical properties of chopped carbon reinforced polymers produced by material extrusion additive manufacturing. Materials, 2019. 12(23): p. 3885.

[10] Fang, L., et al., Data driven analysis of thermal simulations, microstructure and mechanical properties of Inconel 718 thin walls deposited by metal additive manufacturing. arXiv preprint arXiv:2110.07108, 2021.

[11] Bachhar, N., et al., 3D printing of semicrystalline polypropylene: towards eliminating warpage of printed objects. Bulletin of Materials Science, 2020. 43(1): p. 171.

[12] Gordelier, T.J., et al., Optimising the FDM additive manufacturing process to achieve maximum tensile strength: a state-of-the-art review. Rapid Prototyping Journal, 2019. 25(6): p. 953-971.

[13] Yap, Y.L., et al., Material jetting additive manufacturing: An experimental study using designed metrological benchmarks. Precision engineering, 2017. 50: p. 275-285.

[14] Ngo, T.D., et al., Additive manufacturing (3D printing): A review of materials, methods, applications and challenges. Composites Part B: Engineering, 2018. 143: p. 172-196.

[15] Nune, K., et al., Functional response of osteoblasts in functionally gradient titanium alloy mesh arrays processed by 3D additive manufacturing. Colloids and Surfaces B: Biointerfaces, 2017. 150: p. 78-88.

[16] Huang, Y.-M. and C.-P. Jiang, Curl distortion analysis during photopolymerisation of stereolithography using dynamic finite element method. The International Journal of Advanced Manufacturing Technology, 2003. 21: p. 586-595.

[17] Pandzic, a., influence of layer height, build orientation and post curing on tensile mechanical properties of sla 3d printed material. annals of daaam & proceedings, 2021.

[18] Zhou, J.G., D. Herscovici, and C.C. Chen, Parametric process optimization to improve the accuracy of rapid prototyped stereolithography parts. International Journal of Machine Tools and Manufacture, 2000. 40(3): p. 363-379.

[19] Liu, Q., M.C. Leu, and S.M. Schmitt, Rapid prototyping in dentistry: technology and application. The international journal of advanced manufacturing technology, 2006. 29: p. 317-335.

[20] Gibson, I. and D. Shi, Material properties and fabrication parameters in selective laser sintering process. Rapid prototyping journal, 1997. 3(4): p. 129-136.

[21] Williams, J.D. and C.R. Deckard, Advances in modeling the effects of selected parameters on the SLS process. Rapid Prototyping Journal, 1998. 4(2): p. 90-100.

[22] Goodridge, R., C. Tuck, and R. Hague, Laser sintering of polyamides and other polymers. Progress in Materials science, 2012. 57(2): p. 229-267.

[23] Crump, S.S., Apparatus and method for creating three-dimensional objects. 1992, Google Patents.

[24] Zhao, Q., et al., Experimental investigation of shear walls using carbon fiber reinforced polymer bars under cyclic lateral loading. Engineering Structures, 2019. 191: p. 82-91.

[25] Lee, C., et al., Measurement of anisotropic compressive strength of rapid prototyping parts. Journal of materials processing technology, 2007. 187: p. 627-630.

[26] Zein, I., et al., Fused deposition modeling of novel scaffold architectures for tissue engineering applications. Biomaterials, 2002. 23(4): p. 1169-1185.

[27] Gibson, I., et al., Direct digital manufacturing. Additive manufacturing technologies: 3D printing, rapid prototyping, and direct digital manufacturing, 2015: p. 375-397.

[28] Rodríguez-Panes, A., J. Claver, and A.M. Camacho, The influence of manufacturing parameters on the mechanical behaviour of PLA and ABS pieces manufactured by FDM: A comparative analysis. Materials, 2018. 11(8): p. 1333.

[29] Vidakis, N., et al., A comprehensive investigation of the mechanical behavior and the dielectrics of pure polylactic acid (PLA) and PLA with graphene (GnP) in fused deposition modeling (FDM). International Journal of Plastics Technology, 2019. 23(2): p. 195-206.

[30] Shokrieh, M., et al., Effects of thermal cycles on mechanical properties of an optimized polymer concrete. Construction and Building Materials, 2011. 25(8): p. 3540-3549.

[31] El Moumen, A., M. Tarfaoui, and K. Lafdi, Additive manufacturing of polymer composites: Processing and modeling approaches. Composites Part B: Engineering, 2019. 171: p. 166-182.

[32] Saroia, J., et al., A review on 3D printed matrix polymer composites: its potential and future challenges. The international journal of advanced manufacturing technology, 2020. 106: p. 1695-1721.

[33] Hmeidat, N.S., et al., Processing and mechanical characterization of short carbon fiber-reinforced epoxy composites for material extrusion additive manufacturing. Composites Part B: Engineering, 2021. 223: p. 109122.

[34] Thomason, J.L., The influence of fibre length and concentration on the properties of glass fibre reinforced polypropylene: 5. Injection moulded long and short fibre PP. Composites Part A: Applied Science and Manufacturing, 2002. 33(12): p. 1641-1652.

[35] Nawafleh, N. and E. Celik, Additive manufacturing of short fiber reinforced thermoset composites with unprecedented mechanical performance. Additive Manufacturing, 2020. 33: p. 101109.

[36] Ning, F., et al., Additive manufacturing of carbon fiber reinforced thermoplastic composites using fused deposition modeling. Composites Part B: Engineering, 2015. 80: p. 369-378.

[37] Li, Q., et al., Flexural Properties and Fracture Behavior of CF/PEEK in Orthogonal Building Orientation by FDM: Microstructure and Mechanism. Polymers, 2019. 11(4): p. 656.

[38] Ding, Q., et al., Anisotropy of poly (lactic acid)/carbon fiber composites prepared by fused deposition modeling. Journal of Applied Polymer Science, 2020. 137(23): p. 48786.

[39] Sun, B., et al. Fused-Deposition Modeling 3D Printing of Short-Cut Carbon-Fiber-Reinforced PA6 Composites for Strengthening, Toughening, and Light Weighting. Polymers, 2023. 15, DOI: 10.3390/polym15183722.

[40] Compton, B.G. and J.A. Lewis, 3D□printing of lightweight cellular composites. Advanced materials, 2014. 26(34): p. 5930-5935.

[41] Dani, T., et al., Multi objective optimization of built orientation for rapid prototyping of connecting rod. Int J Sci Res Manag, 2013. 1: p. 13-18.

[42] Caminero, M.A., et al., Impact damage resistance of 3D printed continuous fibre reinforced thermoplastic composites using fused deposition modelling. Composites Part B: Engineering, 2018. 148: p. 93-103.

[43] Melenka, G.W., et al., Evaluation and prediction of the tensile properties of continuous fiber-reinforced 3D printed structures. Composite Structures, 2016. 153: p. 866-875.

[44] Matsuzaki, R., et al., Three-dimensional printing of continuous-fiber composites by in-nozzle impregnation. Scientific Reports, 2016. 6(1): p. 23058.

[45] Bettini, P., et al., Fused deposition technique for continuous fiber reinforced thermoplastic. Journal of Materials Engineering and Performance, 2017. 26: p. 843-848.

[46] Wickramasinghe, S., T. Do, and P. Tran, FDM-Based 3D Printing of Polymer and Associated Composite: A Review on Mechanical Properties, Defects and Treatments. Polymers, 2020. 12(7): p. 1529.

[47] Tekinalp, H.L., et al., Highly oriented carbon fiber–polymer composites via additive manufacturing. Composites Science and Technology, 2014. 105: p. 144-150.

[48] Yu, S., et al., Analytical study on the 3D-printed structure and mechanical properties of basalt fiber-reinforced PLA composites using X-ray microscopy. Composites Science and Technology, 2019. 175: p. 18-27.

[49] Standard, A., Standard test methods for flexural properties of unreinforced and reinforced plastics and electrical insulating materials. ASTM D790. Annual book of ASTM standards, 1997.